arXiv:0711.1311v1 [hep-ph] 8 Nov 2007

Top quark rare decays in a two Higgs doublet model for the top

Itzhak Baum

Top quark rare decays in a two Higgs doublet model for the top

Research Thesis

In partial Fulfillment of the

Requirements for the Degree of

Master of Science in Physics

Itzhak Baum

Submitted to the Senate of

the Technion - Israel Institute of Technology

Tishrei, 5767 Haifa September, 2007

I would like to thank my supervisors, Prof. Gad Eilam and Dr. Shaouly Bar-Shalom, for their long patience, and insights, and help, without whom this work would not have been possible. May all students have such guidance.

Contents

1 Introduction **1**

1.1 The two Higgs doublets model 1

1.2 The two Higgs doublets model "for the top" 2

1.3 Rare processes and the $t \to ch$ and $h \to \bar{t}c$ rare decays 3

1.4 Predictions and constraints on the T2HDM 3

2 Yukawa interactions in the T2HDM **5**

3 The flavor-changing sector of the T2HDM **10**

3.1 Charged-Higgs FC Yukawa interactions 10

3.2 Neutral-Higgs FC Yukawa interactions 10

4 Calculations **13**

4.1 One-loop amplitude 13

4.2 Bounds on the parameter space of the T2HDM 13

4.3 From amplitude to BR 15

4.4 Higgs decay BR 16

4.5 Checks of the calculations 16

4.6 Tree-level amplitude 17

5 Results **19**

5.1 Results for the 1-loop top rare decay $t \to cH^0$ 19

5.2 Results for the 1-loop Higgs rare decay $H^0 \to \bar{t}c$ 23

6 Summary **28**

A Higgs potential in two Higgs doublet models **29**

B Feynman rules for two Higgs doublet models **32**

C 1-loop diagrams calculation **35**

D Definition of the n-point integral functions **38**

E Higgs width calculation **39**

F Cancellation of divergences in the 1-loop amplitude **41**

List of Figures

4.1 1-loop Feynman diagrams for $t \rightarrow cH^0$ 14

5.1 (a) 3D plot of $BR(t \rightarrow cH^0)$ in the $m_{H^+} - \tan\beta$ plane in the T2HDM, and (b) the dominant diagram. We set $m_{h^0} = 1000$ GeV and $m_{A^0} = 1200$ GeV. The color scale represents the BR: the blue represents the lowest BR and red the highest. 20
5.2 (a) 3D plot of $BR(t \rightarrow cH^0)$ in the $m_{h^0} - \tan\beta$ plane in the T2HDM, and (b) the dominant diagram. We set $m_{H^+} = 1000$ GeV and $m_{A^0} = 1200$ GeV. 20
5.3 3D plot of $BR(t \rightarrow cH^0)$ in the $m_{A^0} - m_{h^0}$ plane in the T2HDM. We set $m_{H^+} =$ 660 GeV and $\tan\beta = 28$. 21
5.4 The $BR(t \rightarrow cH^0)$ as a function of $\tan\beta$ at various m_{H^+} in the T2HDM. We set $m_{h^0} = 1000$ GeV and $m_{A^0} = 1200$ GeV. "LHC thresh." stands for the limit of the LHC sensitivity at 100 fb^{-1}. 22
5.5 The $BR(t \rightarrow cH^0)$ as a function of m_{H^+} at various $\tan\beta$ in the T2HDM. We set $m_{h^0} = 1000$ GeV and $m_{A^0} = 1200$ GeV. "LHC thresh." stands for the limit of the LHC sensitivity at 100 fb^{-1}. 22
5.6 The SM value for the $BR(H^0 \rightarrow \bar{t}c + \bar{c}t)$ as a function of the Higgs mass, for $\overline{m_b}(\overline{m_b}) = 4.2$ GeV and for $\overline{m_b}(\overline{m_Z}) = 3$ GeV [27]. The BR is not sensitive to m_c. 24
5.7 (a) 3D plot of $BR(H^0 \rightarrow \bar{t}c + \bar{c}t)$ in the $m_{H^+} - \tan\beta$ plane in the T2HDM, and (b) the dominant diagram. We set $m_{h^0} = 1000$ GeV and $m_{A^0} = 1000$ GeV. . . . 24
5.8 The $BR(H^0 \rightarrow \bar{t}c + \bar{c}t)$ as a function of $\tan\beta$ at different m_{H^+} in the T2HDM. We set $m_{h^0} = 1000$ GeV and $m_{A^0} = 1000$ GeV. 25
5.9 The $BR(H^0 \rightarrow \bar{t}c + \bar{c}t)$ as a function of m_{H^+} at different $\tan\beta$ in the T2HDM. We set $m_{h^0} = 1000$ GeV and $m_{A^0} = 1000$ GeV. 25
5.10 (a) 3D plot of $BR(H^0 \rightarrow \bar{t}c + \bar{c}t)$ in the $m_{h^0} - \tan\beta$ plane in the T2HDM, and (b) the dominant diagram. We set $m_{H^+} = 1000$ GeV and $m_{A^0} = 1000$ GeV. . . . 26
5.11 The $BR(H^0 \rightarrow \bar{t}c + \bar{c}t)$ as a function of $\tan\beta$ at different m_{h^0} in the T2HDM. We set $m_{H^+} = 1000$ GeV and $m_{A^0} = 1000$ GeV. 27

B.1 Feynman rules. 33

E.1 The total width of the SM Higgs: leading order approximation compared to corrected width of [16]. 40

List of Tables

5.1 Comparison of the $BR\,(t \rightarrow cH^0)$ within the T2HDM, the 2HDM-II, and the SM. Masses are in units of GeV. 21
5.2 Comparison of $BR\,(H^0 \rightarrow \bar{t}c + \bar{c}t)$ between the T2HDM, the 2HDM-II, and the SM. Masses are in units of GeV. We set $m_{H^0} = 300$, $\alpha = \beta$, and other parameters to their best-fit value of (4.1). 26

B.1 Feynman rules for Yukawa interactions in the T2HDM and in the 2HDM-II. . . 33
B.2 Feynman rules for vector-vector-scalar interactions [5]. 34
B.3 Feynman rules for vector-scalar-scalar interactions [5]. 34
B.4 Feynman rules for triple-scalar interactions [15, 5]. 34

Abstract

The two Higgs doublet model for the top (T2HDM) is a model with two scalar doublets in which the top quark receives a special status. The special status of the top is manifest in the Yukawa potential, by coupling it to the second Higgs doublet, while all other quarks couple to the first Higgs doublet. The working assumption of the model is that the vacuum expectation value (VEV) of the second Higgs (v_2) is much larger than the first Higgs VEV (v_1), so that the top receives a much larger mass than all other quarks in a natural manner, and $\tan\beta \equiv v_2/v_1$ is large. In addition, these Yukawa couplings generate potentially enhanced flavor-changing (FC) interactions, both in the charged and the neutral sectors. These interactions can greatly enhance FC decays such as $t \to ch$ and $h \to \bar{t}c$.

In this work we explicitly (and independently) derive the Yukawa and Higgs potential of the T2HDM, obtaining the scalar to quarks and triple scalar interactions Feynman rules. We calculate the branching ratio (BR) of the one-loop and tree-level rare FC decays $t \to ch$ and $h \to \bar{t}c$ in the T2HDM. We explore the BR within the parameter space of the T2HDM, focusing on regions in which $BR(t \to ch)$ and $BR(h \to \bar{t}c)$ in the T2HDM can be enhanced compared to these BR's in the standard model (SM) and two Higgs doublet models (2HDM) of types I and II. We find that the BR of the rare decays $t \to ch$ and $h \to \bar{t}c$ can be enhanced by many orders of magnitude in the T2HDM compared to the BR in the SM and in the 2HDM-I,II, especially in regions of the parameter space where the decays are dominated by dynamics of the neutral scalar sector.

The $BR(t \to ch)$ can be measured in the upcoming Large Hadron Collider (LHC), if its value is above $\sim 5\times10^{-5}$ which is the discovery threshold of the LHC. We find that the $BR(t \to ch)$ can exceed the LHC threshold in certain regions of the parameter space of the T2HDM, reaching up to $\sim 10^{-4}$. Moreover, we find that the $BR(h \to \bar{t}c)$ in the T2HDM can exceed $\sim 10^{-4}$. Discovering these processes at the LHC will show a clear indication of new physics beyond the standard model, and will particularly motivate the special dynamics of the T2HDM setup.

Chapter 1

Introduction

The standard model (SM) of elementary particles has been highly successful in describing observed and measured phenomena. It contains, however, an unexplored sector, namely, the Higgs sector. The SM also has several problems, one of which is the quark mass hierarchy problem, especially the top quark having a much larger mass than all other quarks.

In its minimal form the SM Higgs sector is comprised of one Higgs doublet, but that is not necessarily the case. Non minimal extensions of the Higgs sector can describe the same observed phenomena, and predict additional phenomena, which are as yet unobserved, but not ruled out. This work will describe one such extension of the SM – the two-Higgs doublet model "for the top" (T2HDM). The T2HDM features particular Yukawa couplings whereby the top quark receives a special status. This particular Yukawa structure also gives rise to potentially large flavor-changing (FC) couplings in the up-quark sector.

In this work we will explicitly (and independently) derive the Yukawa potential of the model, though it has been shown elsewhere [1, 2].

The FC rare decays $t \to ch$ and $h \to \bar{t}c$ have a very low branching ratio (BR) in the SM, of $\sim 10^{-13}$ [3, 4]. This low BR makes these decays extremely sensitive to new physics in the scalar sector. In this work we will explore the BR of the FC rare decays $t \to ch$ and $h \to \bar{t}c$ in the parameter space of the T2HDM, at the 1-loop level (we adhere in this work to the t'Hooft Feynman gauge) and at the tree-level order. We will focus on regions of the parameter space in which the $BR(t \to ch)$ can exceed the detection limit of the upcoming large hadron collider (LHC), and also on regions where the $BR(t \to ch)$ and $BR(h \to \bar{t}c)$ can be enhanced significantly compared to other two Higgs doublet models (2HDM).

1.1 The two Higgs doublets model

The minimal extension of the SM is the two Higgs doublet model (2HDM). A comprehensive review of the principles of the 2HDM can be found in [5]. Basically, the model is comprised of two Higgs doublets, Φ_1 and Φ_2. They usually obey discrete symmetries, whose aim is to define the Yukawa terms, and which divide them into several types. The 3 most common types are: type I, where Φ_2 couples to all quarks, and Φ_1 does not couple to quarks; type II, where Φ_1 couples to down quarks, and Φ_2 couples to up quarks; type III, which denotes a general case in which both Φ_1 and Φ_2 couple to all quarks.

The type II 2HDM describes the Yukawa structure of the minimal supersymmetric standard model (MSSM), and is therefore of particular interest in the literature.

Several properties are common to all types of 2HDM. All feature additional physical scalars: initially there are two complex doublets, hence 8 (2×4) degrees of freedom, and the electroweak breaking absorbs 3. We are therefore left with 5 degrees of freedom which are equivalent to 5 physical scalars, plus the 3 (unphysical) Goldstone bosons which are present also in the minimal

SM, and which are "eaten" by the gauge bosons. The components of the scalar doublets mix to produce the mass eigenstates. They are denoted as follows: h^0, H^0 – CP-even neutral scalars, A^0 – CP-odd neutral scalar, G^0 – neutral (unphysical) Goldstone boson, $H^\pm$ – charged scalars, $G^\pm$ – charged (unphysical) Goldstone bosons. The mixing conserves the symmetries of the theory: the mass matrix does not mix scalars with different charges, and in CP conserving theories there is no mixing between CP-even and CP-odd scalars.

1.2 The two Higgs doublets model "for the top"

The 2HDM "for the top" (T2HDM) was first introduced by Das and Kao [1] as an effective approach for providing the top its mass in a natural way. They proposed a 2HDM in which the second Higgs field couples only to the top, while the first Higgs field couples to all other quarks.

The choice of the coupling can be expressed also in terms of a discrete symmetry imposed on the Lagrangian [1], under which the fields transform as follows:

$$\begin{aligned} &\Phi_1 \rightarrow -\Phi_1, \qquad d_R \rightarrow -d_R, \quad u_R \rightarrow -u_R \; (u = u, c), \\ &\Phi_2 \rightarrow +\Phi_2, \qquad Q_L \rightarrow +Q_L, \quad t_R \rightarrow +t_R \end{aligned} \tag{1.1}$$

where: Φ_i are the Higgs fields, $(u, c, t)_R$ are the right-handed $SU(2)$ singlet up-type quarks, $d_R = (d, s, b)_R$ are the down-type right-handed quarks, and Q_L is the left-handed $SU(2)$ quark doublet. The discrete symmetry (1.1) produces the Yukawa couplings of the T2HDM, described below. This discrete symmetry is softly broken by the λ_5 term of (2.2) as discussed in [6].

With these Yukawa couplings, the top gets its mass primarily from the second Higgs vacuum expectation value (VEV), which we will choose to be much larger than the first Higgs VEV:

$$\frac{v_2}{v_1} \gg 1. \tag{1.2}$$

This is the working assumption of the T2HDM.

This particular Yukawa coupling can also give rise to large FC interactions, as we shall later show.

Distinct features of the T2HDM are:

- The $H^+\bar{c}b$ vertex is enhanced by the ratio of CKM matrix elements V_{tb}/V_{cb} compared to other 2HDM's. This property motivated our work, as well as the analysis in [7, 8].
- There are tree-level FC interactions in the up-quark sector; but there are no tree-level FC interactions in the down-quark sector, unlike the case of the 2HDM-III in which the tree-level FC interactions are both in the up and down-quark sectors.
- The couplings of the neutral scalars (H^0, h^0, A^0) to all the quarks except for the top quark, increase with $\tan\beta$. This property motivated the analysis in [9].

These points will be further elaborated upon in Sec. 3.

The T2HDM could stand on its own, although the couplings and symmetries defined above do not seem "naturally derived". However, it could also be viewed as an effective low energy realization of a more fundamental theory. Some examples are:

- An extra-dimensions scenario, Randall-Sundrum like, in which the couplings are derived from the location of fields in the 5th dimension [10].

- A technicolor scenario with a topcolor condensate scalar having a large VEV, which by construction couples only to the top quark [11].

- A non-minimal supersymmetry scenario, in which Φ_1 couples to down quarks and Φ_2 to up quarks, but the couplings for u_R, c_R are very small, and get most of their value from loop corrections.

1.3 Rare processes and the $t \to ch$ and $h \to \bar{t}c$ rare decays

Rare decays are a sensitive probe for new physics [12]. Such decays are defined as rare because in the SM they are subject to a suppression mechanism, which can be either highly effective cancellations, such as the GIM mechanism, or the conservation of a fundamental symmetry, such as lepton number.

New physics models may greatly enhance such processes, by working around the suppression mechanism. For example, the process $\mu \to e\gamma$ which is forbidden by lepton flavor conservation, can be realized by relaxing the symmetry in the neutrino sector (see e.g. [13]).

In this work, we have chosen to explore the BR of the rare decays $h \to \bar{t}c$ and $t \to ch$ in the T2HDM, as a potential new-physics signal at the LHC. The LHC discovery limit for the $t \to ch$ decay process is $BR \geq 5.8 \cdot 10^{-5}$ [14] for an integrated luminosity of $100 fb^{-1}$. As mentioned before, the SM BR is about $\sim 10^{-13}$, and, therefore, unobservable at the LHC. Previous studies [15] have shown that the $BR(t \to ch)$, where $h = H^0, h^0, A^0$, could reach up to $\sim 10^{-4}$ in the 2HDM type II and in the MSSM, and about $\sim 10^{-6}$ in the 2HDM type I.

In the T2HDM the FC decays can be enhanced due to the large H^+cb coupling which is proportional to $V_{tb} \times \tan\beta$ instead of $V_{cb} \times \tan\beta$ in other 2HDM's, as we shall later show. This large coupling motivated us in calculating the BR of $t \to ch$.

As an aside, we will briefly recall how the experimental detection of the process will proceed at the LHC [14]. At the LHC the top will be mainly produced in $t\bar{t}$ pairs. One then searches for processes in which the t decays to ch, while the $\bar{t}$ decays in the main $\bar{b}W^-$channel. The h is most likely to decay into $b\bar{b}$ pairs when its mass is below 130 GeV, whereas above this mass the W^+W^- decay channel starts to dominate [16]. The full process (in the lower mass range) will look like: $gg \to t\bar{t} \to hc\bar{b}W^- \to b\bar{b}c\bar{b}l\bar{\nu}$. The main background will come from a similar process in which the $t \to bW^+ \to bjc$ (where j denotes a quark jet), and the $\bar{t}$ decays as before. In this case a misidentification of the jet as $\bar{b}$ will result in an erroneous $t \to ch$ identification [14].

The $h \to \bar{t}c$ decay is the complementary process to $t \to ch$ if $m_h > m_t + m_c$. The amplitude of the process is equal to the amplitude of $t \to ch$, by applying crossing symmetry [17], and therefore it is subject to the same enhancements as the $t \to ch$ process, compared with other 2HDM's and the SM.

1.4 Predictions and constraints on the T2HDM

To date several rare decays and other observables have been calculated in the T2HDM:

- The electric dipole moment (EDM) of the electron was calculated in the T2HDM [1], and the neutron EDM in [18], for their dependence on the CP violating mixing in the Higgs sector. The experimental results constrain this mixing.

- The process $b \to s\gamma$ was calculated in the T2HDM in the leading order, for its contribution to $C_{7,8}$ [19, 20]. By adding this result to the SM prediction one can compare the theory to the experimental result: $BR(b \to s\gamma) = (3.55 \pm 0.26) \times 10^{-4}$ [21], and derive bounds on the model. A prediction was also given for the partial rate asymmetry of the decay, which is very different from the SM prediction, and can be measured in B factories. Newer measurements in [21] seem to further restrict the additional CP violating phase in the Yukawa sector of the T2HDM (see below).

- The meson mixings $B-\bar{B}$ [22], $K-\bar{K}$ [8], $D-\bar{D}$ [8, 1] were calculated for contributions to the mass splittings $\Delta m_{B,K,D}$, ϵ_K of $K-\bar{K}$ mixing, the ratio p/q of $D-\bar{D}$ mixing. These results further constrain the parameter space of the T2HDM, in a manner similar to $b \to s\gamma$, as was discussed above, ruling out different regions of the parameter space [1, 8, 22].

- The process $b \to s l_i^+ l_j^-$ was calculated in [23], and was found to constrain the T2HDM weakly, so that those bounds are included within other calculated bounds.

- The process $gq \to qqq$ was considered in [9], where q denotes a b or c quark. It was found that the T2HDM cross section for this process will be detectable at the LHC, while the MSSM and the 2HDM type II are not expected to have a detectable signal. Therefore if such a signal is observed at the LHC then it will stand out as a clear indication in favor of the T2HDM.

- The process $Z \to b\bar{s} + \bar{b}s$ was calculated in various models [7]. Experimentally the BR has a weak upper bound. It was found that the T2HDM BR for this decay is comparable in size to the SM predicted value ($\sim 10^{-8}$), and to the MSSM with $\tilde{t}-\tilde{c}$ mixing. In comparison, MSSM with $\tilde{b}-\tilde{s}$ mixing is about two orders of magnitude higher, while the 2HDM type II is about two orders of magnitude lower.

- In a recent article [2] some of the above calculations were simultaneously combined for a fit to recent experimental data, mostly from B-factories. The best-fit values and 1σ intervals for all the parameters in the fit were calculated. As this is the most comprehensive work constraining the T2HDM parameters, these were the bounds used in the present work.

The rare decays $t \to ch$ and $h \to \bar{t}c$ have not been calculated yet in the T2HDM. This work is aimed at this calculation, with the intention of giving a prediction which will hopefully be verifiable at the LHC.

Chapter 2

Yukawa interactions in the T2HDM

In this section we give an explicit derivation of the Feynman rules of scalar-quark-quark interactions in the T2HDM. We will start from the interaction-basis Lagrangian, which follows from the symmetries imposed. We will rotate the quark fields and the scalar fields to their mass basis. Finally, we will write the Yukawa terms in the mass basis, arranged by interactions, in terms of standard parameters.
The Lagrangian density of the T2HDM Yukawa interactions is of the following form [1]:

$$\mathcal{L}_Y = -\bar{Q}_{Li}\Phi_1 F_{ij} d_{Rj} - \bar{Q}_{Li}\tilde{\Phi}_1 G_{ij=1,2} \begin{pmatrix} u \\ c \end{pmatrix}_R - \bar{Q}_{Li}\tilde{\Phi}_2 G_{i3} t_R + h.c. \ , \tag{2.1}$$

where: $i,j = 1,2,3$ are flavour indices, $L(R) \equiv \left(1-(+)\gamma^5\right)/2$ are the chiral left (right) projection operators, $f_{L(R)} = L(R)f$ are left(right)-handed fermion fields, F, G are general 3×3 Yukawa matrices, and:

$$\Phi = \begin{pmatrix} \Phi^+ \\ \frac{v+\Phi^0}{\sqrt{2}} \end{pmatrix}, \quad \tilde{\Phi} = \begin{pmatrix} \frac{v^*+\Phi^{0*}}{\sqrt{2}} \\ -\Phi^- \end{pmatrix} \ .$$

The Higgs potential can be generically written as (assuming CP conservation) [5]:

$$\begin{aligned} \mathcal{L}_H &= \lambda_1\left(\Phi_1^+\Phi_1 - v_1^2/2\right)^2 + \lambda_2\left(\Phi_2^+\Phi_2 - v_2^2/2\right)^2 + \lambda_3\left[\left(\Phi_1^+\Phi_1 - v_1^2/2\right) + \left(\Phi_2^+\Phi_2 - v_2^2/2\right)\right]^2 + \\ &\quad + \lambda_4\left[\left(\Phi_1^+\Phi_1\right)\left(\Phi_2^+\Phi_2\right) - \left(\Phi_1^+\Phi_2\right)\left(\Phi_2^+\Phi_1\right)\right] + \lambda_5\left|\Phi_1^+\Phi_2 - v_1 v_2/2\right|^2 \ . \end{aligned} \tag{2.2}$$

The absence of CP violation implies that the CP-even and CP-odd Higgs mass-eigenstates do not mix, and that the VEV's can be taken to be real without affecting the Lagrangian of the theory [5].
Dropping the flavor indices and defining: $\mathbb{I}^{(12)} = \mathrm{diag}(1,1,0)$, $\mathbb{I}^{(3)} = \mathrm{diag}(0,0,1)$, the Yukawa potential reads:

$$\mathcal{L}_Y \ = \ -\bar{Q}_L\Phi_1 F d_R - \bar{Q}_L\left(\tilde{\Phi}_1 G\mathbb{I}^{(12)} + \tilde{\Phi}_2 G\mathbb{I}^{(3)}\right)u_R + h.c. \ . \tag{2.3}$$

Inserting Φ, $\tilde{\Phi}$ into the Yukawa potential and rearranging the Yukawa terms:

$$\begin{aligned}
\mathcal{L}_Y &= -\bar{d}_L \frac{v_1}{\sqrt{2}} F d_R - \bar{u}_{Li} \frac{1}{\sqrt{2}} \left(v_1 G \mathbb{I}^{(12)} + v_2 G \mathbb{I}^{(3)}\right) u_R - \bar{Q}_L \Phi_1 F d_R - \\
&\quad -\bar{Q}_L \left(\tilde{\Phi}_1 G \mathbb{I}^{(12)} + \tilde{\Phi}_2 G \mathbb{I}^{(3)}\right) u_R - \frac{v_2^*}{v_1^*} \bar{Q}_{Li} \tilde{\Phi}_1 G_{i3} t_R + \frac{v_2^*}{v_1^*} \bar{Q}_{Li} \tilde{\Phi}_1 G_{i3} t_R + h.c. = \\
&= -\bar{d}_L \frac{v_1}{\sqrt{2}} F d_R - \bar{u}_L \frac{1}{\sqrt{2}} \left(v_1 G \mathbb{I}^{(12)} + v_2 G \mathbb{I}^{(3)}\right) u_R - \bar{Q}_L \Phi_1 F d_R - \\
&\quad -\bar{Q}_L \left(\tilde{\Phi}_1 G \mathbb{I}^{(12)} + \frac{v_2}{v_1} \tilde{\Phi}_1 G \mathbb{I}^{(3)}\right) u_R - \bar{Q}_{Li} \left(\tilde{\Phi}_2 - \frac{v_2}{v_1} \tilde{\Phi}_1\right) G_{i3} t_R + h.c. = \\
&= -\bar{d}_L \frac{v_1}{\sqrt{2}} F d_R - \bar{u}_L \frac{1}{\sqrt{2}} \left(v_1 G \mathbb{I}^{(12)} + v_2 G \mathbb{I}^{(3)}\right) u_R - \bar{d}_L \frac{1}{\sqrt{2}} \Phi_1^0 F d_R - \bar{u}_L \Phi_1^+ F d_R + \\
&\quad -\bar{u}_L \frac{1}{\sqrt{2}} \Phi_1^{0*} G \left(\mathbb{I}^{(12)} + \frac{v_2}{v_1} \mathbb{I}^{(3)}\right) u_R + \bar{d}_L \Phi_1^- G \left(\mathbb{I}^{(12)} + \frac{v_2}{v_1} \mathbb{I}^{(3)}\right) u_R + \\
&\quad -\bar{u}_L \frac{1}{\sqrt{2}} \left(\Phi_2^{0*} - \frac{v_2}{v_1} \Phi_1^{0*}\right) G \mathbb{I}^{(3)} t_R + \bar{d}_L \left(\Phi_2^- - \frac{v_2}{v_1} \Phi_1^-\right) G \mathbb{I}^{(3)} t_R + h.c.\ . \qquad (2.4)
\end{aligned}$$

If the G_{ij} are of $O(1)$, and v_2 is much larger than v_1, then the eigenvalues of the matrix $\left(v_1 G \mathbb{I}^{(12)} + v_2 G \mathbb{I}^{(3)}\right)$ can be expanded as a series of v_1/v_2. After expanding to the leading order, the mass matrix eigenvalues are: $O(1) \cdot [v_1, v_1, v_2]$. As can be seen, the top quark receives a mass contribution from the second, and larger, VEV, while the up and charm receive their masses from the first VEV.

Rotating to the quark mass basis, we define: $d_{L,R} \to D_{L,R} d_{L,R}$, $u_{L,R} \to U_{L,R} u_{L,R}$, such that:

$$\begin{aligned}
M_d &\equiv \frac{v_1}{\sqrt{2}} D_L^\dagger F D_R = \mathrm{diag}\left(m_d, m_s, m_b\right), \\
M_u &\equiv U_L^\dagger \frac{1}{\sqrt{2}} \left(v_1 G \mathbb{I}^{(12)} + v_2 G \mathbb{I}^{(3)}\right) U_R = \mathrm{diag}\left(m_u, m_c, m_t\right). \qquad (2.5)
\end{aligned}$$

We define the CKM matrix: $V_{CKM} \equiv U_L^\dagger D_L$, $V_{CKM}^\dagger \equiv D_L^\dagger U_L$ (we will henceforward drop the subscript CKM when referring to the CKM matrix), and a new mixing matrix for the up-quarks:

$$\Sigma \equiv M_u U_R^\dagger \mathbb{I}^{(3)} U_R, \qquad (2.6)$$

as was originally defined in [1].

The matrix U_R can be generally parametrized by multiplying 3 rotation matrices [8]. Defining 3 rotation angles: $\alpha_{12} = \phi$, $\alpha_{23} = \sin^{-1}\left(\epsilon_{ct}\xi\right)$ and $\alpha_{13} = \sin^{-1}\left(\epsilon_{ct}\xi'\right)$, where $\epsilon_{ct} \equiv \frac{m_c}{m_t}$, and ξ, ξ' are parameters naturally of $O(1)$, and $\xi \equiv |\xi|^{i\varphi_\xi}$, we get:

$$\begin{aligned}
U_R = &\begin{pmatrix} \cos\phi & -\sin\phi & 0 \\ \sin\phi & \cos\phi & 0 \\ 0 & 0 & 1 \end{pmatrix} \begin{pmatrix} 1 & 0 & 0 \\ 0 & \sqrt{1-|\epsilon_{ct}\xi|^2} & -\epsilon_{ct}\xi^* \\ 0 & \epsilon_{ct}\xi & \sqrt{1-|\epsilon_{ct}\xi|^2} \end{pmatrix} \begin{pmatrix} \sqrt{1-|\epsilon_{ct}\xi'|^2} & 0 & -\epsilon_{ct}\xi'^* \\ 0 & 1 & 0 \\ \epsilon_{ct}\xi' & 0 & \sqrt{1-|\epsilon_{ct}\xi'|^2} \end{pmatrix} = \\
&= \begin{pmatrix} * & * & * \\ * & * & * \\ \epsilon_{ct}\xi'\sqrt{1-|\epsilon_{ct}\xi|^2} & \epsilon_{ct}\xi & \sqrt{1-|\epsilon_{ct}\xi|^2}\sqrt{1-|\epsilon_{ct}\xi'|^2} \end{pmatrix}, \qquad (2.7)
\end{aligned}$$

where the asterisks $(*)$ denote terms which are not relevant for our calculations to follow.

Using Eq. (2.7) we can now write the Σ matrix:

$$\frac{\Sigma}{m_t} = \left(\begin{array}{ccc} \frac{m_u}{m_t}\epsilon_{ct}^2 \left|\xi'\right|^2 \left(1-\left|\epsilon_{ct}\xi\right|^2\right) & \frac{m_u}{m_t}\epsilon_{ct}^2 \xi'^* \xi \sqrt{1-\left|\epsilon_{ct}\xi\right|^2} & \frac{m_u}{m_t}\epsilon_{ct}\xi'^* \left(1-\left|\epsilon_{ct}\xi\right|^2\right) \sqrt{1-\left|\epsilon_{ct}\xi'\right|^2} \\ \epsilon_{ct}^3 \xi^* \xi' \sqrt{1-\left|\epsilon_{ct}\xi\right|^2} & \epsilon_{ct}^3 \left|\xi\right|^2 & \epsilon_{ct}^2 \xi^* \sqrt{1-\left|\epsilon_{ct}\xi\right|^2} \sqrt{1-\left|\epsilon_{ct}\xi'\right|^2} \\ \epsilon_{ct}\xi' \left(1-\left|\epsilon_{ct}\xi\right|^2\right) \sqrt{1-\left|\epsilon_{ct}\xi'\right|^2} & \epsilon_{ct}\xi \sqrt{1-\left|\epsilon_{ct}\xi\right|^2} \sqrt{1-\left|\epsilon_{ct}\xi'\right|^2} & \left(1-\left|\epsilon_{ct}\xi\right|^2\right) \left(1-\left|\epsilon_{ct}\xi'\right|^2\right) \end{array} \right). \tag{2.8}$$

The special mixing matrix between up and down quarks via the charged Higgs, neglecting terms of $O\left(\epsilon_{ct}^2\right)$ or $O\left(\frac{m_u}{m_t}\right)$ (recall: $\epsilon_{ct} \equiv \frac{m_c}{m_t}$), can then be written approximately as:

$$\left(\Sigma^\dagger V\right)/m_t = \left(\begin{array}{ccc} \epsilon_{ct}\xi'^* V_{td} & \epsilon_{ct}^3 \xi'^* \xi V_{cs} + \epsilon_{ct}\xi'^* V_{ts} & \epsilon_{ct}\xi'^* V_{tb} \\ \epsilon_{ct}\xi^* V_{td} & \epsilon_{ct}^3 \left|\xi\right|^2 V_{cs} + \epsilon_{ct}\xi^* V_{ts} & \epsilon_{ct}\xi^* V_{tb} \\ V_{td} & \epsilon_{ct}^2 \xi V_{cs} + V_{ts} & V_{tb} - V_{tb}\epsilon_{ct}^2 \left(\left|\xi\right|^2 + \left|\xi'\right|^2\right) \end{array} \right). \tag{2.9}$$

We note that the matrix was approximated for the purpose of illustration. In all calculations the matrix was used without neglecting anything.

The Yukawa terms in the quark mass basis are:

$$\begin{aligned} \mathcal{L}_Y \;=\; & -\bar{d}_L M_d d_R - \bar{u}_L M_u u_R - \bar{d}_L \Phi_1^0 \frac{M_d}{v_1} d_R - \bar{u}_L \Phi_1^{0*} \frac{M_u}{v_1} u_R - \\ & -\bar{u}_L U_L^\dagger \Phi_1^+ D_L D_L^\dagger F D_R d_R + \bar{d}_L D_L^\dagger \Phi_1^- U_L U_L^\dagger \frac{1}{v_1} \left(v_1 G \mathbb{I}^{(12)} + v_2 G \mathbb{I}^{(3)}\right) U_R u_R - \\ & -\bar{u}_L U_L^\dagger \frac{1}{\sqrt{2}} \left(\Phi_2^{0*} - \frac{v_2}{v_1}\Phi_1^{0*}\right) G \mathbb{I}^{(3)} U_R u_R + \bar{d}_L D_L^\dagger \left(\Phi_2^- - \frac{v_2}{v_1}\Phi_1^-\right) U_L U_L^\dagger G \mathbb{I}^{(3)} U_R u_R + h.c.\ . \end{aligned} \tag{2.10}$$

We will henceforward drop the mass terms.

Using: $\mathbb{I}^{(12)} \cdot \mathbb{I}^{(3)} = [0]^{3\times 3}$, and: $U_L^\dagger G \mathbb{I}^{(3)} U_R = U_L^\dagger \frac{1}{v_2} \left(v_1 G \mathbb{I}^{(12)} + v_2 G \mathbb{I}^{(3)}\right) U_R U_R^\dagger \mathbb{I}^{(3)} U_R = \frac{\sqrt{2}}{v_2}\Sigma$, we get:

$$\begin{aligned} \mathcal{L}_Y \;=\; & -\bar{d}_L \Phi_1^0 \frac{M_d}{v_1} d_R - \bar{u}_L \Phi_1^{0*} \frac{M_u}{v_1} u_R - \Phi_1^+ \bar{u}_L V \frac{\sqrt{2} M_d}{v_1} d_R + \Phi_1^- \bar{d}_L V_{CKM}^\dagger \frac{\sqrt{2} M_u}{v_1} u_R - \\ & - \left(\Phi_2^{0*} - \frac{v_2}{v_1}\Phi_1^{0*}\right) \bar{u}_L \frac{1}{v_2} \Sigma u_R + \left(\Phi_2^- - \frac{v_2}{v_1}\Phi_1^-\right) \bar{d}_L V^\dagger \frac{\sqrt{2}}{v_2} \Sigma u_R + h.c.\ . \end{aligned} \tag{2.11}$$

The Higgs fields are not in their mass basis yet. The mass basis is derived from the Higgs potential in the Lagrangian, see App. A (see also [5]).

We note that the real parts of the neutral Higgs fields generally rotate with the angle α, whereas the other Higgs fields rotate with the angle β. This is due to their shift by the VEV's. This point is sometimes overlooked in the literature, where often the value for α is chosen arbitrarily. This omission of α can perhaps be attributed to the MSSM, where the angle α is constrained by the Higgs masses [5].

The Higgs fields in the mass basis are defined as follows:

$$\begin{aligned} & \Phi^0 = \Phi^{0r} + i\Phi^{0i}, \qquad \tan(\beta) \equiv \frac{v_2}{v_1}, \\ & \Phi_1^{or} = H^0 \cos\alpha - h^0 \sin\alpha, \qquad \Phi_1^{oi} = G^0 \cos\beta - A^0 \sin\beta, \qquad \Phi_1^+ = G^+ \cos\beta - H^+ \sin\beta, \\ & \Phi_2^{or} = H^0 \sin\alpha + h^0 \cos\alpha, \qquad \Phi_2^{oi} = G^0 \sin\beta + A^0 \cos\beta, \qquad \Phi_2^+ = G^+ \sin\beta + H^+ \cos\beta. \end{aligned} \tag{2.12}$$

The Yukawa terms in the quark and Higgs mass basis, are then:

$$\begin{aligned}
\mathcal{L}_Y &= -\bar{d}_L\left[\left(H^0\cos\alpha-h^0\sin\alpha\right)+i\left(G^0\cos\beta-A^0\sin\beta\right)\right]\frac{M_d}{v_1}d_R- \\
&\quad -\bar{u}_L\left[\left(H^0\cos\alpha-h^0\sin\alpha\right)-i\left(G^0\cos\beta-A^0\sin\beta\right)\right]\frac{M_u}{v_1}u_R- \\
&\quad -\left(G^+\cos\beta-H^+\sin\beta\right)\bar{u}_LV\frac{\sqrt{2}M_d}{v_1}d_R+\left(G^-\cos\beta-H^-\sin\beta\right)\bar{d}_LV^\dagger\frac{\sqrt{2}M_u}{v_1}u_R- \\
&\quad -\left[\left(H^0\sin\alpha+\phi_2^{0r}\cos\alpha\right)-i\left(G^0\sin\beta+A^0\cos\beta\right)\right]\bar{u}_L\frac{1}{v_2}\Sigma u_R+ \\
&\quad +\frac{v_2}{v_1}\left[\left(H^0\cos\alpha-\phi_2^{0r*}\sin\alpha\right)-i\left(G^0\cos\beta-A^0\sin\beta\right)\right]\bar{u}_L\frac{1}{v_2}\Sigma u_R+ \\
&\quad +\left[\left(G^-\sin\beta+H^-\cos\beta\right)-\frac{v_2}{v_1}\left(G^-\cos\beta-H^-\sin\beta\right)\right]\bar{d}_LV^\dagger\frac{\sqrt{2}}{v_2}\Sigma u_R+h.c.\ . \qquad (2.13)
\end{aligned}$$

Collecting identical interactions:

$$\begin{aligned}
\mathcal{L}_Y &= -\bar{d}_L\left[\left(H^0\cos\alpha-h^0\sin\alpha\right)+i\left(G^0\cos\beta-A^0\sin\beta\right)\right]\frac{M_d}{v_1}d_R+ \\
&\quad +H^0\bar{u}_L\left[-\frac{M_u}{v_1}\cos\alpha-\frac{1}{v_2}\Sigma\sin\alpha+\frac{1}{v_1}\Sigma\cos\alpha\right]u_R+ \\
&\quad +h^0\bar{u}_L\left[\frac{M_u}{v_1^*}\sin\alpha-\frac{1}{v_2}\Sigma\cos\alpha-\frac{1}{v_1}\Sigma\sin\alpha\right]u_R+ \\
&\quad +iG^0\bar{u}_L\left[\frac{M_u}{v_1}\cos\beta+\frac{1}{v_2}\Sigma\sin\beta-\frac{1}{v_1}\Sigma\cos\beta\right]u_R+ \\
&\quad +iA^0\bar{u}_L\left[-\frac{M_u}{v_1}\sin\beta+\frac{1}{v_2}\Sigma\cos\beta+\frac{1}{v_1}\Sigma\sin\beta\right]u_R+ \\
&\quad +\left(-G^+\cos\beta+H^+\sin\beta\right)\bar{u}_LV\frac{\sqrt{2}M_d}{v_1}d_R+ \\
&\quad +G^-\bar{d}_LV^\dagger\left[\cos\beta\frac{\sqrt{2}M_u}{v_1}+\sin\beta\frac{\sqrt{2}}{v_2}\Sigma-\cos\beta\frac{\sqrt{2}}{v_1}\Sigma\right]u_R+ \\
&\quad +H^-\bar{d}_LV^\dagger\left[-\sin\beta\frac{\sqrt{2}M_u}{v_1}+\cos\beta\frac{\sqrt{2}}{v_2}\Sigma+\sin\beta\frac{\sqrt{2}}{v_1}\Sigma\right]u_R+h.c.\ . \qquad (2.14)
\end{aligned}$$

Using: $v_1=v\cos\beta$, $v_2=v\sin\beta$, $v=\sqrt{v_1^2+v_2^2}=\frac{2m_W}{g}$, and adding the h.c., we get the final

Yukawa terms, in the physical mass basis, arranged by interactions:

$$\begin{aligned}\mathcal{L}_Y =& H^0\bar{d}\left[-\frac{gM_d}{2m_W}\frac{\cos\alpha}{\cos\beta}\right]d + h^0\bar{d}\left[\frac{gM_d}{2m_W}\frac{\sin\alpha}{\cos\beta}\right]d+\\
&+ A^0\bar{d}\left[i\frac{gM_d}{2m_W}\tan\beta\,(R-L)\right]d + G^0\bar{d}\left[-i\frac{gM_d}{2m_W}\,(R-L)\right]d+\\
&+ H^0\bar{u}\left[\frac{g}{2m_W}\left(-M_u\frac{\cos\alpha}{\cos\beta}+\Sigma\left(-\frac{\sin\alpha}{\sin\beta}+\frac{\cos\alpha}{\cos\beta}\right)\right)R+(h.c.)\,L\right]u+\\
&+ h^0\bar{u}\left[\frac{g}{2m_W}\left(M_u\frac{\sin\alpha}{\cos\beta}-\Sigma\left(\frac{\cos\alpha}{\sin\beta}+\frac{\sin\alpha}{\cos\beta}\right)\right)R+(h.c.)\,L\right]u+\\
&+ A^0\bar{u}\left[i\frac{g}{2m_W}\left(-M_u\tan\beta+\Sigma\left(\tan\beta+\cot\beta\right)\right)R+(h.c.)\,L\right]u + G^0\bar{u}\left[i\frac{gM_u}{2m_W}\,(R-L)\right]u+\\
&+ G^+\bar{u}\frac{g}{\sqrt{2}m_W}\left[-VM_dR+M_uVL\right]d+h.c.+\\
&+ H^+\bar{u}\frac{g}{\sqrt{2}m_W}\left[\tan\beta VM_dR+\left(-M_u\tan\beta+\Sigma^\dagger\left(\tan\beta+\cot\beta\right)\right)VL\right]d+h.c.\;.\end{aligned}\tag{2.15}$$

For completeness, in App. B we give the complete list of Feynman rules for the T2HDM model, as derived above.

Chapter 3

The flavor-changing sector of the T2HDM

The T2HDM features unique flavor-changing (FC) couplings of both charged Higgs and neutral Higgs, where the neutral Higgs FC couplings are in the up-quark sector only. These couplings can enhance FC processes, in particular the $t \to ch$ decay.

3.1 Charged-Higgs FC Yukawa interactions

In the SM the leading order diagrams of the $t \to ch$ decay are at the 1-loop level, through the mediation of W^+ gauge bosons and b-quarks in the loop, being $\propto V_{cb}$. In general, in any 2HDM there is a corresponding vertex of $H^+\bar{c}b$, and the process $t \to ch$ proceeds also via similar diagrams with H^+ and b in the loop. In the T2HDM the $H^+\bar{c}b$ vertex receives a particular value distinct from other 2HDM's:

$$
\begin{aligned}
L \supset{}& \frac{g}{\sqrt{2}m_W} H^+ \bar{c} \left[\tan\beta V M_d R + \left(-M_u \tan\beta + \Sigma^\dagger \left(\tan\beta + \cot\beta\right)\right) V L\right]_{cb} b \sim \\
\sim{}& \frac{g}{\sqrt{2}m_W} H^+ \bar{c} \left[\tan\beta V_{cb} m_b R + m_c \left(-\tan\beta V_{cb} + \xi^* \left(\tan\beta + \cot\beta\right) V_{tb}\right) L\right] b \; . \qquad (3.1)
\end{aligned}
$$

As can be seen, the $H^+\bar{c}b$ vertex has a term proportional to $V_{cb} \times \tan\beta$ which is common to other 2HDM's, but has an additional term proportional to $(\tan\beta + \cot\beta) \times \left(\Sigma^\dagger V\right)_{cb} \sim m_c \xi^* V_{tb}$, as shown above in (2.9). The main contribution for 1-loop diagrams with internal H^+ and b, in the T2HDM, will therefore come from $m_c \xi^* V_{tb}$ terms, and is thus not CKM suppressed.
For our analysis we also consider the $H^+\bar{t}b$ vertex in the T2HDM:

$$
\begin{aligned}
L \supset{}& \frac{g}{\sqrt{2}m_W} H^+ \bar{t} \left\{\tan\beta V_{tb} m_b R + \right. \\
&+ \left. \left[-m_t V_{tb} \tan\beta + m_t \left(V_{tb} - V_{tb}\epsilon_{ct}^2 \left(|\xi|^2 + |\xi'|^2\right)\right)\left(\tan\beta + \cot\beta\right)\right] L \right\} b = \\
={}& \frac{g}{\sqrt{2}m_W} H^+ \bar{t} \left\{\tan\beta V_{tb} m_b R + \right. \\
&+ \left. \left[m_t V_{tb} \cot\beta - m_t V_{tb} \epsilon_{ct}^2 \left(|\xi|^2 + |\xi'|^2\right)\left(\tan\beta + \cot\beta\right)\right] L \right\} b \qquad (3.2)
\end{aligned}
$$

We can see that by taking $\xi, \xi' \to 0$ the $H^+\bar{t}b$ interaction in (3.2) becomes equivalent to that of a 2HDM type I or II.

3.2 Neutral-Higgs FC Yukawa interactions

A priori there is no distinction between h^0 and H^0 other than the rotation angle α. In this work we therefore adopt $\alpha = \beta$, and in the following discussion we explore the consequences of this choice, in particular the elimination of the tree-level $H^0\bar{t}c$ vertex.

The $t \to cH^0$ decay in the T2HDM can proceed at tree level, from the following interaction term (see Sec. 2):

$$\begin{aligned} L \supset H^0 \bar{t} & \left[\frac{g}{2m_W} \left(-M_u \frac{\cos\alpha}{\cos\beta} + \Sigma \left(-\frac{\sin\alpha}{\sin\beta} + \frac{\cos\alpha}{\cos\beta} \right) \right) R + (h.c.)\, L \right]_{tc} c \sim \\ \sim H^0 \bar{t} & \left[\frac{g}{2m_W} \left(-\frac{\sin\alpha}{\sin\beta} + \frac{\cos\alpha}{\cos\beta} \right) (m_c \xi R + m_c \epsilon_{ct} \xi L) \right] c, \end{aligned} \tag{3.3}$$

where we used the off-diagonal terms of Σ from Eq. 2.8, neglecting terms of order ϵ_{ct}^2 (recall $\epsilon_{ct} = m_c/m_t$), $\Sigma_{tc} \sim m_c \xi$ and $\left(\Sigma^\dagger\right)_{tc} \sim m_c \epsilon_{ct} \xi$.
For arbitrary α and β, this will lead to $t \to cH^0$ decay at tree level. On the other hand, the $H^0 \bar{t} c$ vertex can vanish if:
1)$\xi = 0$,
2)$-\frac{\sin\alpha}{\sin\beta} + \frac{\cos\alpha}{\cos\beta} = 0 \quad \Leftrightarrow \quad \alpha = \beta + n\pi$.
In this work we wish to examine the case of a vanishing $H^0 \bar{t} c$ tree-level interaction, therefore adopting $\alpha = \beta$, since:

1. $\xi = 0$ is strongly disfavoured by the bounds in [2], as we will discuss in Sec. 4.2.
2. $\xi = 0$ cancels the potentially enhanced term of the $H^+ \bar{c} b$ coupling, as shown above.
3. The limit $\alpha = \beta$ is a natural result of the MSSM, when the mass of the CP-odd neutral Higgs, A^0, is large (see e.g. [5] in the limit $m_{A^0} \to \infty$). Note that $\alpha = \beta$ is widely used in the literature, partly for this reason. Even though the T2HDM setup is not natural within the MSSM, this will help us compare our results with other existing results in different types of 2HDM's.
4. The limit $\alpha = \beta$ sets the scalar H^0 to be SM-like. As such, it will have SM-Higgs Yukawa couplings:

   $$\mathcal{L}_Y^{\alpha=\beta} \supset H^0 \bar{d} \left[-\frac{g M_d}{2m_W} \right] d + H^0 \bar{u} \left[-\frac{g M_u}{2m_W} \right] u \ . \tag{3.4}$$

   In that case, the direct mass bounds on the SM Higgs may roughly apply to H^0.

We turn now to the h^0-up quarks Yukawa interactions. The 1-loop $t \to cH^0$ can proceed also through the mediation of h^0 scalars and top quarks in the loop. In these diagrams the important interactions are the $h^0 \bar{t} c$ and the $h^0 \bar{t} t$ vertices, which get special values in the T2HDM.
The $h^0 \bar{t} c$ interaction reads:

$$\begin{aligned} L \supset h^0 \bar{t} & \left[\frac{g}{2m_W} \left(M_u \frac{\sin\alpha}{\cos\beta} - \Sigma \left(\frac{\cos\alpha}{\sin\beta} + \frac{\sin\alpha}{\cos\beta} \right) \right) R + (h.c.)\, L \right]_{tc} c \sim \\ \sim h^0 \bar{t} & \left[-\frac{g}{2m_W} \left(\frac{\cos\alpha}{\sin\beta} + \frac{\sin\alpha}{\cos\beta} \right) (m_c \xi R + m_c \epsilon_{ct} \xi L) \right] c, \end{aligned} \tag{3.5}$$

where setting $\alpha = \beta$ gives:

$$\mathcal{L}^{\alpha=\beta} \supset h^0 \bar{t} \left[-\frac{g}{2m_W} (\tan\beta + \cot\beta) (m_c \xi R + m_c \epsilon_{ct} \xi L) \right] c. \tag{3.6}$$

One can see that the $h^0 \bar{t} c$ interaction can be enhanced by $\tan\beta$.

The $h^0\bar{t}t$ interaction, with $\alpha = \beta$, reads:

$$\begin{aligned} L \supset\ & h^0\bar{t}\left\{\frac{g}{2m_W}\left[m_t \tan\beta - \Sigma_{tt}\left(\tan\beta + \cot\beta\right)\right]R + (h.c.)\,L\right\}t \sim \\ \sim\ & h^0\bar{t}\left\{\frac{g}{2m_W}\left[-m_t \cot\beta + m_c\epsilon_{ct}\left(\left|\xi\right|^2 + \left|\xi'\right|^2\right)\left(\tan\beta + \cot\beta\right)\right]R + (h.c.)\,L\right\}t, \end{aligned} \tag{3.7}$$

where we use $\Sigma_{tt} = \left(\Sigma^\dagger\right)_{tt} \sim m_t - m_c\epsilon_{ct}\left(\left|\xi\right|^2 + \left|\xi'\right|^2\right)$. As in the case of $H^+\bar{t}b$, the leading term $\propto m_t \tan\beta$ cancels, leaving terms that are suppressed either by ϵ_{ct}^2 or $\cot^2\beta$.

Chapter 4

Calculations

4.1 One-loop amplitude

The 1-loop decay amplitude is composed of 10 Feynman diagrams, shown in Fig. 4.1. Their explicit calculation is given in App. C.
The calculation was aimed to be model-independent. Thus, the Feynman diagrams in Fig. 4.1 were drawn by assuming general vertices, which are defined in Fig. B.1 in App. C, and by assuming general fields:
q_i– denotes a quark (up or down type)
V_α– denotes vector (gauge) fields
H_α– denotes scalar fields
In this way it was possible to calculate the same process in different models, by inserting the appropriate vertices and fields.
The 1-loop integrals were calculated numerically with FORTRAN using the FF package [24].
The calculations were done using the Passarino-Veltman reduction scheme, which expresses the integrals in terms of basic scalar n-point functions. All other (vector, tensor) integrals can be computed using combinations of the scalar functions (for explicit furmulae see e.g. [15] App. A). In App. D we give the definitions of the reduced functions that we used to calculate the 1-loop integrals.

4.2 Bounds on the parameter space of the T2HDM

As was mentioned in the introduction, bounds on the T2HDM charged-sector parameter space were simultaneously calculated in [2] to give a best fit to various experimental results. The processes that were selected were the ones most sensitive to the T2HDM.
We describe here the processes for which the parameter fit was done in [2], and summarize in Eq. (4.1) the allowed values of the parameters of the T2HDM at 1σ.

- The BR of $B \to X_s\gamma$ [20] was estimated from the shifts in the Wilson coefficients $C_{7,8}$ caused by the T2HDM. The BR constrains mainly the parameters m_{H^+}, $\tan\beta$ and ξ.
- The BR of $B^+ \to \tau^+\nu_\tau$ was calculated in the T2HDM [2]. This process receives a tree-level contribution from charged-Higgs exchange, and has a large impact in constraining the parameter space, especially m_{H^+} and ξ'.
- The CP-violating parameter ε_K was calculated in the T2HDM [8], and was found in [2] to severely constrain the parameters m_{H^+}, $\tan\beta$ and ξ.
- The time dependent amplitude of the CP asymmetry $a_{\Psi K} = A\left(\bar{B}^0 \to J/\psi K_s\right)$, was found to constrain the parameters m_{H^+} and $\tan\beta$.

$t \to c\,h$ *diagrams*

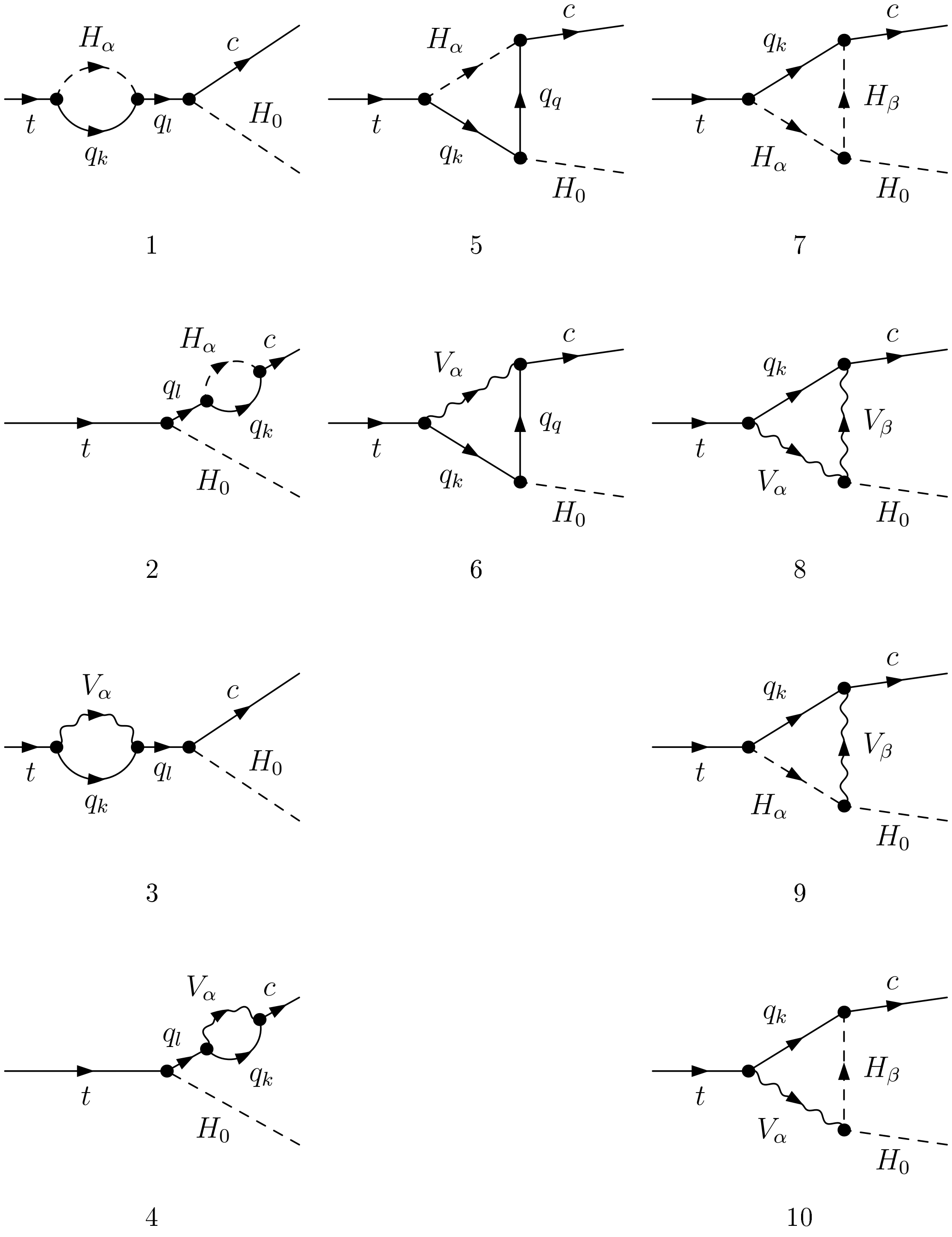

Figure 4.1: 1-loop Feynman diagrams for $t \to cH^0$

- The neutron EDM constrains mainly m_{H^+}, $\tan\beta$ and ξ'.
- The Δm_D mass difference from $D-\bar{D}$ mixing can be completely dominated by NP effects, and so it was required in the analysis that the T2HDM value would not exceed the experimental value. This requirement constrains m_{H^+}, $\tan\beta$, ξ and ξ'.
- The ratio $\Delta m_{B_s}/\Delta m_{B_d}$ was included in the fit, although it gave weaker constraints than ε_K.

In the analysis of [2], a χ^2 function was defined, that featured as variables the T2HDM charged Higgs sector parameters – $\tan\beta$, m_H^+, ξ and ξ' and the SM CKM-matrix parameters – ρ, η and $[\alpha,\beta,\gamma]$ (unitarity triangle). These parameters were simultaneously fit to the processes described above. As this is the most comprehensive work constraining the T2HDM parameters, these were the bounds used in the present work. Since they are directly relevant to the present work, we list the final results of [2] below (recall that $\xi = |\xi|\, e^{i\varphi_\xi}$):

$$\begin{aligned}
m_{H^\pm} &= \left(660^{+390}_{-280}\right)\ \text{GeV}, \\
\tan\beta &= 28^{+44}_{-8}, \\
|\xi| &\sim 0.8, \quad 0.5<|\xi|<1, \\
\varphi_\xi &= \left(110^{+30}_{-65}\right)^\circ, \\
|\xi'| &\sim 0.21, \\
\varphi_{\xi'} &\sim 250^\circ.
\end{aligned} \tag{4.1}$$

We note that these values are also allowed for the 2HDM-II as given in [25]. We further note that the Δm_D mass difference from $D-\bar{D}$ mixing receives a contribution from the neutral sector that can constrain the neutral sector parameters, but that contribution is suppressed by a factor of $\left(\frac{1}{\tan\beta}\frac{m_c}{m_t}\frac{m_{H^+}}{m_{h^0}}\right)^2$ compared to the charged Higgs contribution, and therefore does not impose significant constraints on the parameter space of the neutral sector [26, 8].

Direct constraints from experiments impose weak bounds [27]: for the SM Higgs, the direct search bound is $m_{H^0} > 114$ GeV. For supersymmetry, bounds for neutral scalars are $m_h > 90$ GeV, while for charged scalars current bounds are $m_{H^+} > 80$ GeV.

4.3 From amplitude to BR

From the amplitude we get the width of the decay using [27]:

$$\Gamma = 4\pi\cdot\lambda^{\frac{1}{2}}\left(1,\frac{m_c^2}{m_t^2},\frac{m_h^2}{m_t^2}\right)\cdot\frac{\sum\limits_{pol}\overline{|\mathcal{M}|^2}}{64\pi^2 m_t}\,, \tag{4.2}$$

where $\sum\limits_{pol}\overline{|\mathcal{M}|^2}$ is the squared amplitude averaged over initial polarizations and summed over final polarizations, and $\lambda(x,y,z) = x^2+y^2+z^2-2xy-2xz-2yz$. In the case of an incoming fermion, we have: $\sum\limits_{pol}\overline{|\mathcal{M}|^2} = \frac{1}{2}\sum\limits_{pol}|\mathcal{M}|^2$.

Calculating the squared amplitude, we get:

$$
\begin{aligned}
\mathcal{M} &= \frac{i\bar{u}_c}{16\pi^2}\left(M_L L + M_R R\right) u_t, \\
\sum_{pol} |\mathcal{M}|^2 &= \frac{1}{256\pi^4} tr\left[\bar{u}_c\left(M_L L + M_R R\right) u_t \bar{u}_t \left(M_R^* L + M_L^* R\right) u_c\right] = \\
&= \frac{1}{256\pi^4}\left[2m_c m_t\left(M_L M_R^* + M_R M_L^*\right) + \left(m_c^2 + m_t^2 - m_h^2\right)\left(M_L M_L^* + M_R M_R^*\right)\right].
\end{aligned}
\tag{4.3}
$$

The BR is then:

$$
BR\left(t \to ch\right) = \frac{\Gamma\left(t \to ch\right)}{\sum\limits_x \Gamma\left(t \to x\right)} \,. \tag{4.4}
$$

Where usually only $x = W^+b$ is taken, since its BR is very close to 1 [27]. We take the tree-level value of $\Gamma\left(t \to W^+b\right) = 1.55$ GeV. If the mass of the H^+ is smaller than the mass of the top, the process $t \to H^+b$ is possible and significant, and must be taken into account in the sum.

4.4 Higgs decay BR

The 1-loop amplitude of the opposite process, $h \to \bar{t}c + \bar{c}t$, is identical to the 1-loop amplitude of $t \to ch$, by applying crossing symmetry [17]. The width of the process is given by:

$$
\Gamma\left(h \to \bar{t}c + \bar{c}t\right) = 2 \times \Gamma\left(h \to \bar{t}c\right) = 2N_c \lambda^{\frac{1}{2}}\left(1, \frac{m_c^2}{m_h^2}, \frac{m_t^2}{m_h^2}\right) \cdot \frac{\sum\limits_{pol}\overline{|\mathcal{M}|^2}}{16\pi m_h}, \tag{4.5}
$$

where $N_c = 3$ is the color factor, and $\sum\limits_{pol}\overline{|\mathcal{M}|^2} = \sum\limits_{pol}|\mathcal{M}|^2$ in this case (an incoming scalar).
In order to calculate the BR for $h \to \bar{t}c$, one has to calculate the total width of the scalars. In this work we have included leading-order contributions to the Higgs width from $h \to \bar{q}q$, $h \to VV$, $h \to 2$ scalars and $h \to$ vector+scalar [28]. The last can be important in some regions of the parameter space such as low $\tan\beta$. The formulae used for the calculation of the total width are given in App. E, along with a plot of the SM Higgs width in the leading order approximation compared with higher order predictions, in Fig. E.1.

4.5 Checks of the calculations

- We have successfully reproduced the results for $BR(t \to ch)$ obtained in [3] in the SM and in [15] in the 2HDM-II.
- We have successfully reproduced the results for $BR\left(h \to \bar{t}c\right)$ obtained in [4] in the SM and in [25] in the 2HDM-II. We note that Arhrib's results matched for $\alpha_{EW} \sim 1/128.9$, which is different from the one reportedly used, $\alpha_{EW} \sim 1/137$, as also confirmed by him in a private communication. However, we were not able to reproduce the $BR\left(h \to \bar{t}c\right)$ values of [15], as also stated in [25].
- Some amplitudes have a divergent part. Since the process is calculated at leading order, no renormalization is needed to cancel the divergent terms, and they should cancel among themselves. This cancellation is demonstrated in App. F analytically. It was also verified numerically in the FORTRAN code. Checking that the results do not diverge is also a test of the self-consistency of the 1-loop amplitude calculations.

4.6 Tree-level amplitude

As stated in the introduction, there are FC tree-level interactions of h^0 in the T2HDM, when $\alpha = \beta$, as opposed to H^0 which has no FC tree-level interactions when $\alpha = \beta$. Therefore, the decays $t \to ch^0$ and $h^0 \to \bar{t}c$ at tree-level are possible when allowed kinematically. The tree-level coupling $h^0\bar{t}c$ was given in Sec. 3. Here we derive the leading order tree-level BR values of these two decays. We will neglect throughout the derivation terms of order: m_c^2/m_t^2, m_b^2/m_t^2, $m_c^2/m_{h^0}^2$ and $\cot^2\beta$. The last term is neglected in accordance with the working assumption of the T2HDM, which is a large $\tan\beta$. We also set $\alpha = \beta$. The last requirement is not imperative, but it renders simpler formulae and makes the following derivation consistent with the 1-loop calculations of $t \to cH^0$ and $H^0 \to \bar{t}c$ decays in this work.
The tree-level amplitude for the process $t \to ch^0$ is:

$$\mathcal{M}\left(t \to ch^0\right) = \bar{u}_c\left[\frac{g}{2m_W}\left(\left(M_u\right)_{ct}\frac{\sin\alpha}{\cos\beta} - \Sigma_{ct}\left(\frac{\cos\alpha}{\sin\beta} + \frac{\sin\alpha}{\cos\beta}\right)\right)R + (h.c.)\,L\right]u_t, \tag{4.6}$$

where from (2.8) we have:

$$\begin{aligned}\Sigma_{ct} &= m_t\epsilon_{ct}^2\xi^*\sqrt{1-|\epsilon_{ct}\xi|^2}\sqrt{1-|\epsilon_{ct}\xi'|^2} \sim m_c\epsilon_{ct}\xi^*,\\ \left(\Sigma^\dagger\right)_{ct} &= m_t\epsilon_{ct}\xi^*\sqrt{1-|\epsilon_{ct}\xi|^2}\sqrt{1-|\epsilon_{ct}\xi'|^2} \sim m_c\xi^*,\end{aligned} \tag{4.7}$$

which we insert in the amplitude with $\alpha = \beta$ to get:

$$\begin{aligned}\mathcal{M}\left(t \to ch^0\right) &= \bar{u}_c\frac{-g}{2m_W}\left(\cot\beta + \tan\beta\right)m_c\xi^*\left[\epsilon_{ct}R + L\right]_{ct}u_t \equiv\\ &\equiv \bar{u}_c\left[M_R R + M_L L\right]u_t.\end{aligned} \tag{4.8}$$

The squared amplitude summed over external spinors is:

$$\begin{aligned}\sum_{pol}|\mathcal{M}|^2 &= 2m_c m_t\left(M_L M_R^* + M_R M_L^*\right) + \left(m_t^2 + m_c^2 - m_h^2\right)\left(M_L M_L^* + M_R M_R^*\right) =\\ &= \left[\frac{g^2 m_c^2}{4m_W^2}\left(\cot\beta + \tan\beta\right)^2|\xi|^2\right]\left[2m_c m_t\cdot 2\epsilon_{ct} + \left(m_t^2 + m_c^2 - m_{h^0}^2\right)\left(1 + \epsilon_{ct}^2\right)\right] \sim\\ &\sim \frac{g^2 m_c^2}{4m_W^2}\tan^2\beta\,|\xi|^2\left[m_t^2 - m_{h^0}^2\right].\end{aligned} \tag{4.9}$$

From $\sum\limits_{pol}\overline{|\mathcal{M}|^2} = \frac{1}{2}\sum\limits_{pol}|\mathcal{M}|^2$ we can calculate the BR's of the processes $t \to ch^0$ and $h^0 \to \bar{t}c$.
The width of $t \to ch^0$ reads:

$$\begin{aligned}\Gamma\left(t \to ch^0\right) &= 4\pi\cdot\lambda^{\frac{1}{2}}\left(1, \frac{m_c^2}{m_t^2}, \frac{m_{h^0}^2}{m_t^2}\right)\cdot\frac{\sum\limits_{pol}\overline{|\mathcal{M}|^2}}{64\pi^2 m_t} \sim\\ &\sim \frac{g^2|\xi|^2 m_t m_c^2}{128\pi m_W^2}\tan^2\beta\left(1 - \frac{m_{h^0}^2}{m_t^2}\right)^2.\end{aligned} \tag{4.10}$$

The width for $t \to bW^+$ (at tree-level and neglecting terms of order m_b^2/m_t^2 and α_s) is [27]:

$$\Gamma\left(t \to bW^+\right) \sim \frac{g^2 m_t}{64\pi}\left(1 - \frac{m_W^2}{m_t^2}\right)\left(1 - 2\frac{m_W^2}{m_t^2} + \frac{m_t^2}{m_W^2}\right), \tag{4.11}$$

from which we get the leading order $BR\left(t\rightarrow ch^0\right)$ (for large $\tan\beta$):

$$BR\left(t\rightarrow ch^{0}\right)\sim\frac{\left|\xi\right|^{2}m_{c}^{2}}{2m_{W}^{2}}\tan^{2}\beta\left(1-\frac{m_{h^{0}}^{2}}{m_{t}^{2}}\right)^{2}\left(1-\frac{m_{W}^{2}}{m_{t}^{2}}\right)^{-1}\left(1-2\frac{m_{W}^{2}}{m_{t}^{2}}+\frac{m_{t}^{2}}{m_{W}^{2}}\right)^{-1}. \tag{4.12}$$

For instance, for the best-fit parameters of Eq. (4.1), $\tan\beta=28$, $|\xi|=0.8$, and for $\alpha=\beta$, and $m_{h^0}=91$ GeV, we get $BR\left(t\rightarrow ch^0\right)=0.0077$.
By applying crossing symmetry on $\left|\mathcal{M}\right|^2$, the tree-level squared amplitude of the opposite process, $h^0\rightarrow\bar{t}c$, is:

$$\sum_{pol}\overline{\left|\mathcal{M}\right|^{2}}\sim\frac{g^{2}m_{c}^{2}}{4m_{W}^{2}}\tan^{2}\beta\left|\xi\right|^{2}\left[m_{h^{0}}^{2}-m_{t}^{2}\right], \tag{4.13}$$

from which we get:

$$\begin{aligned}\Gamma\left(h\rightarrow\bar{t}c+\bar{c}t\right)=2\times\Gamma\left(h^{0}\rightarrow\bar{t}c\right)&=2N_{c}\lambda^{\frac{1}{2}}\left(1,\frac{m_{c}^{2}}{m_{h^{0}}^{2}},\frac{m_{t}^{2}}{m_{h^{0}}^{2}}\right)\cdot\frac{\sum_{pol}\overline{\left|\mathcal{M}\right|^{2}}}{16\pi m_{h^{0}}}\sim\\&\sim\frac{N_{c}\left|\xi\right|^{2}g^{2}m_{h^{0}}m_{c}^{2}}{32\pi m_{W}^{2}}\tan^{2}\beta\left(1-\frac{m_{t}^{2}}{m_{h^{0}}^{2}}\right)^{2}.\end{aligned} \tag{4.14}$$

For $\alpha=\beta$, (assuming also that $m_{h^0}<2m_{A^0},2m_{H^+}$) the total width of h^0 is mainly comprised of fermion decays, since the couplings $W^+W^-h^0$, $Z^0Z^0h^0$ and $H^0H^0h^0$ are all $\propto\sin\left(\beta-\alpha\right)$ (see table B.2 and App. E). Below the $t\bar{t}$ threshold (at about 340 GeV) the $b\bar{b}$ decays dominate. The width of $h^0\rightarrow\bar{b}b$ is then (see App. E):

$$\Gamma\left(h^{0}\rightarrow\bar{b}b\right)\sim\frac{N_{c}g^{2}m_{b}^{2}m_{h^{0}}}{32\pi m_{W}^{2}}\tan^{2}\beta. \tag{4.15}$$

In this case, the BR of $h^0\rightarrow\bar{t}c$ is:

$$BR\left(h^{0}\rightarrow\bar{t}c+\bar{c}t\right)\sim\left|\xi\right|^{2}\frac{m_{c}^{2}}{m_{b}^{2}}\left(1-\frac{m_{t}^{2}}{m_{h^{0}}^{2}}\right)^{2}. \tag{4.16}$$

For $|\xi|=0.8$ and $m_{h^0}=300$ GeV, we get $BR\left(h^0\rightarrow\bar{t}c+\bar{c}t\right)=0.023$.

Chapter 5

Results

In this section we give our results and discussion for the 1-loop decays $BR\left(t \to cH^0\right)$ and $BR\left(H^0 \to \bar{t}c\right)$ in the T2HDM. All the masses are in units of GeV. We set $\alpha = \beta$ for the reasons explained above. Other parameters are set to their best-fit value of (4.1) unless stated otherwise. Our calculations were done in the t'Hooft Feynman gauge. The SM Higgs has a best-fit mass to EW precision data of 91^{+45}_{-32} GeV [27]. In our setup in which H^0 has couplings identical to the SM Higgs, we expect these bounds to be roughly applicable, and therefore we set $m_{H^0} = 91$ GeV in the process $t \to cH^0$. We take the total t-quark width $\Gamma\left(t \to W^+ b\right) = 1.55$ GeV. For the process $H^0 \to \bar{t}c$ we arbitrarily choose $m_{H^0} = 300$ GeV.
For definiteness, other values we used for the calculations were [27]: $m_t = 172.5$ GeV (pole mass), $m_c = \overline{m}_c\left(\overline{m}_c\right) = 1.24$ GeV, $m_b = \overline{m}_b\left(\overline{m}_b\right) = 4.20$ GeV (m_c and m_b are in the $\overline{MS}$ renormalization scheme), $m_W = 80.40$ GeV, $m_Z = 91.188$ GeV, $\cos\theta_W = m_W/m_Z$, $\alpha_{EW}\left(m_z\right) = 1/127.9$. The values were used as given here, without running in energy scale. The BR results were found to be sensitive to m_c and m_b: for example, for the BR value 5.99×10^{-5} quoted in table 5.1 in the upper row for the T2HDM with $m_b = 4.2$ and $m_c = 1.25$, setting $m_b(m_Z) \sim 3$ and $m_c(m_Z) \sim 0.7$ [29] yields 1.28×10^{-5}. We note that our results were not sensitive to m_s.
We used $m_{A^0} = 1000$ GeV to enhance the triple-scalar coupling which is roughly $\propto m_{A^0}^2$, as can be seen in App. A and B. The ξ and ξ' parameters are set to their best-fit value of Eq. (4.1): $|\xi| = 0.8$, $\varphi_\xi = 110°$, $|\xi'| = 0.21$, and $\varphi_{\xi'} = 250°$.

5.1 Results for the 1-loop top rare decay $t \to cH^0$

In Fig. (5.1 a) we show a 3D plot of $BR\left(t \to cH^0\right)$ in the $m_{H^+} - \tan\beta$ plane in the T2HDM. The flat grid in Figs. 5.1 and 5.2 is the LHC detection limit of $BR > 5 \cdot 10^{-5}$, so that the colored surface above the grid is the region in the parameter space which has (in the T2HDM) a BR high enough to be detected at the LHC.
The choice $m_{h^0} = 1000$ GeV in Fig. 5.1 suppresses the diagrams in which the neutral h^0 Higgs runs in the loop and, thus, better explores the charged Higgs sector properties. As expected the BR rises with $\tan\beta$ and is highest when m_{H^+} is lowest. The dominant Feynman diagram in this case is the one which has two H^+ scalars and a b quark in the loop, and is shown in Fig. (5.1 b). This diagram receives an enhancement from the 3-scalar vertex, as discussed above.
In Fig. 5.2 we show the BR in the $m_{h^0} - \tan\beta$ plane in the T2HDM.
We took $m_{H^+} = 1000$ GeV in Fig. 5.2 so that the diagrams in which the charged H^+ Higgs runs in the loop will be suppressed, to better explore the neutral Higgs sector properties. As we can see, the BR is highest when m_{h^0} is lowest, and rises with $\tan\beta$. The dominant diagrams in this case are the ones which have two h^0 or two H^+ scalars in the loop: The diagram with two h^0 dominates in the low $\tan\beta$ – low m_{h^0} region, while the diagram with two H^+ dominates in the high $\tan\beta$ – high m_{h^0} region, and is responsible for the rise of the BR with $\tan\beta$. Both of

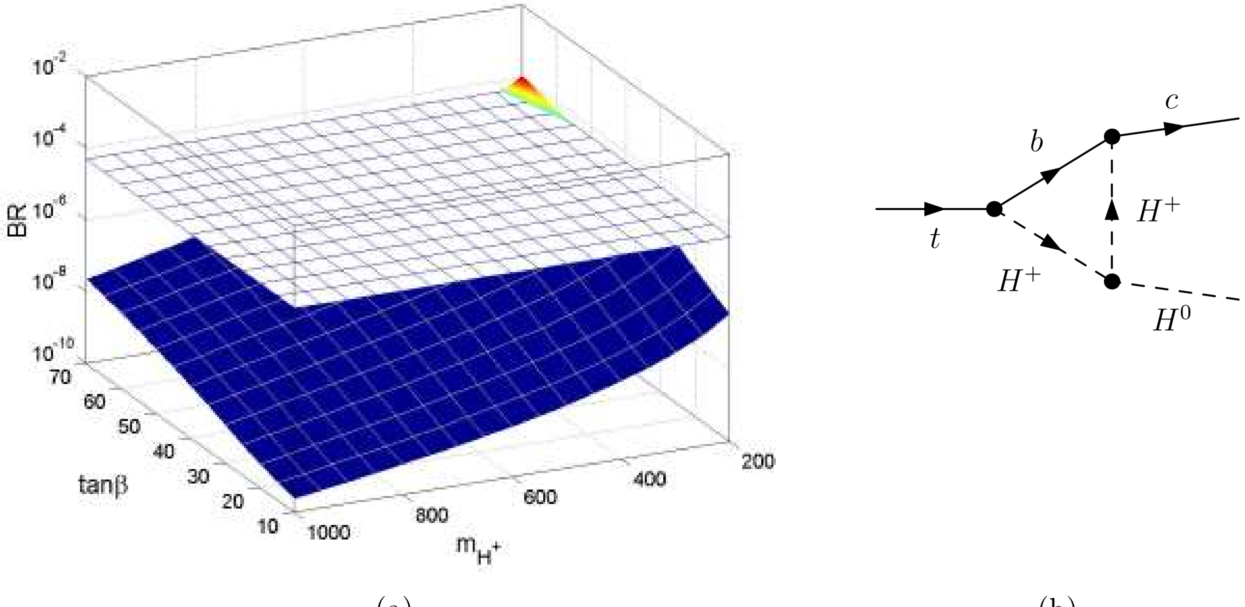

(a) (b)

Figure 5.1: (a) 3D plot of $BR\,(t \to cH^0)$ in the $m_{H^+} - \tan\beta$ plane in the T2HDM, and (b) the dominant diagram. We set $m_{h^0} = 1000$ GeV and $m_{A^0} = 1200$ GeV. The color scale represents the BR: the blue represents the lowest BR and red the highest.

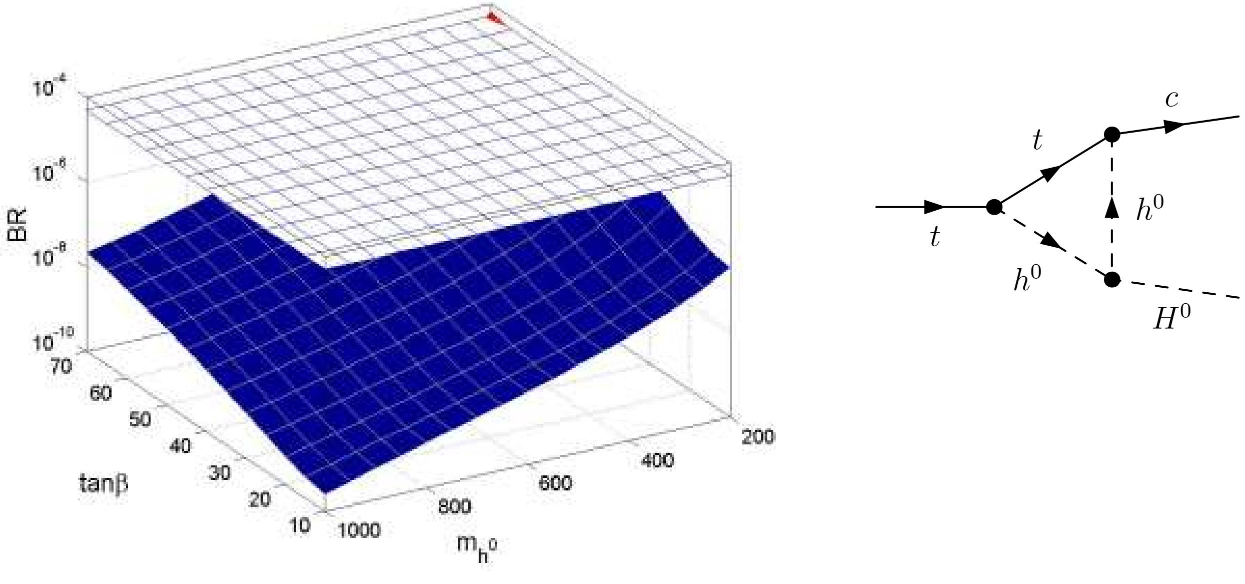

(a) (b)

Figure 5.2: (a) 3D plot of $BR\,(t \to cH^0)$ in the $m_{h^0} - \tan\beta$ plane in the T2HDM, and (b) the dominant diagram. We set $m_{H^+} = 1000$ GeV and $m_{A^0} = 1200$ GeV.

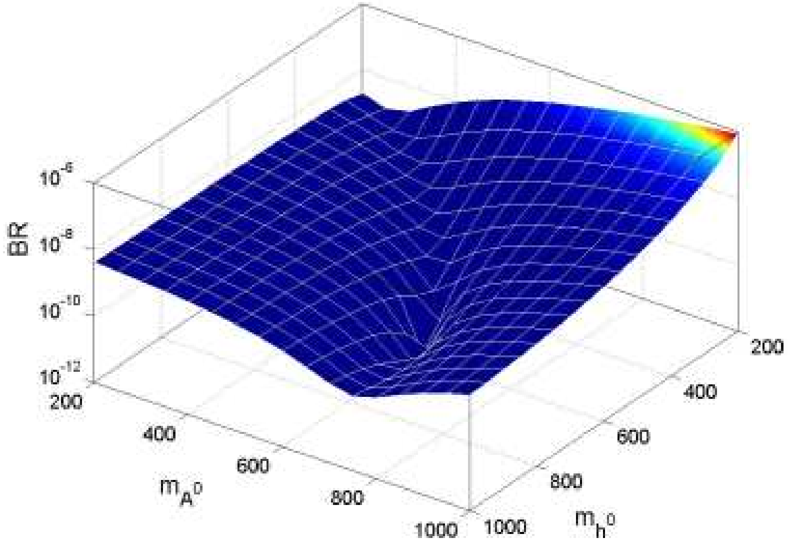

Figure 5.3: 3D plot of $BR\left(t \rightarrow c H^{0}\right)$ in the $m_{A^{0}}-m_{h^{0}}$ plane in the T2HDM. We set $m_{H^{+}}=$ 660 GeV and $\tan \beta=28$.

parameters	SM	2HDM-II	T2HDM
$m_{h^{0}}=800$, $m_{A^{0}}=1000$, $\tan \beta=72$, $m_{H^{+}}=200$	6.03×10^{-14}	4.25×10^{-5}	5.99×10^{-5}
$m_{h^{0}}=800$, $m_{A^{0}}=1000$, $\tan \beta=72$, $m_{H^{+}}=380$	6.03×10^{-14}	1.79×10^{-6}	2.57×10^{-6}
$m_{h^{0}}=200$, $m_{A^{0}}=4000$, $\tan \beta=20$, $m_{H^{+}}=1050$	6.03×10^{-14}	5.15×10^{-8}	9.39×10^{-5}
$m_{h^{0}}=200$, $m_{A^{0}}=1000$, $\tan \beta=20$, $m_{H^{+}}=1050$	6.03×10^{-14}	3.34×10^{-12}	3.14×10^{-7}

Table 5.1: Comparison of the $BR\left(t \rightarrow c H^{0}\right)$ within the T2HDM, the 2HDM-II, and the SM. Masses are in units of GeV.

these diagrams receive an enhancement from the 3-scalar vertex with large $m_{A^{0}}$, as mentioned above.

The plots are similar, yet the BR are higher when the H^{+} runs in the loop. That is a distinctive property of the T2HDM: the charged Higgs coupling $H^{+} \bar{b} c$ can be enhanced by as much as V_{tb} / V_{cb} compared with any other 2HDM.

In Fig. 5.3 we show the BR in the $m_{A^{0}}-m_{h^{0}}$ plane in the T2HDM, at the best fit of the charged sector parameters. The graph shows that the BR rises when $m_{A^{0}}$ is highest and $m_{h^{0}}$ lowest, since then the diagram with two $m_{h^{0}}$ starts to dominate. The dip in the middle of the surface is due to cancellation in the $H^{0} H^{+} H^{+}$ vertex.

In Figs. 5.4 and 5.5 we give 2D plots of the BR as a function of $\tan \beta$ and $m_{H^{+}}$ respectively, with the same parameters as in Fig. 5.1. We can now see the dependence of the BR on $\tan \beta$ and $m_{H^{+}}$ more clearly: the BR rises with $\tan \beta$ but increases with smaller $m_{H^{+}}$.

Finally, we wish to illustrate more clearly the difference between the T2HDM, the 2HDM-II, and the SM. For that purpose we give in table 5.1 the $BR\left(t \rightarrow c H^{0}\right)$ values within these 3 different models, for several points in the relevant parameter space. We recall that the 2HDM-II has a Yukawa potential similar to the MSSM, and has no tree-level FC interactions.

The first two rows illustrate the impact of the charged sector, by setting a high $m_{h^{0}}$. The BR

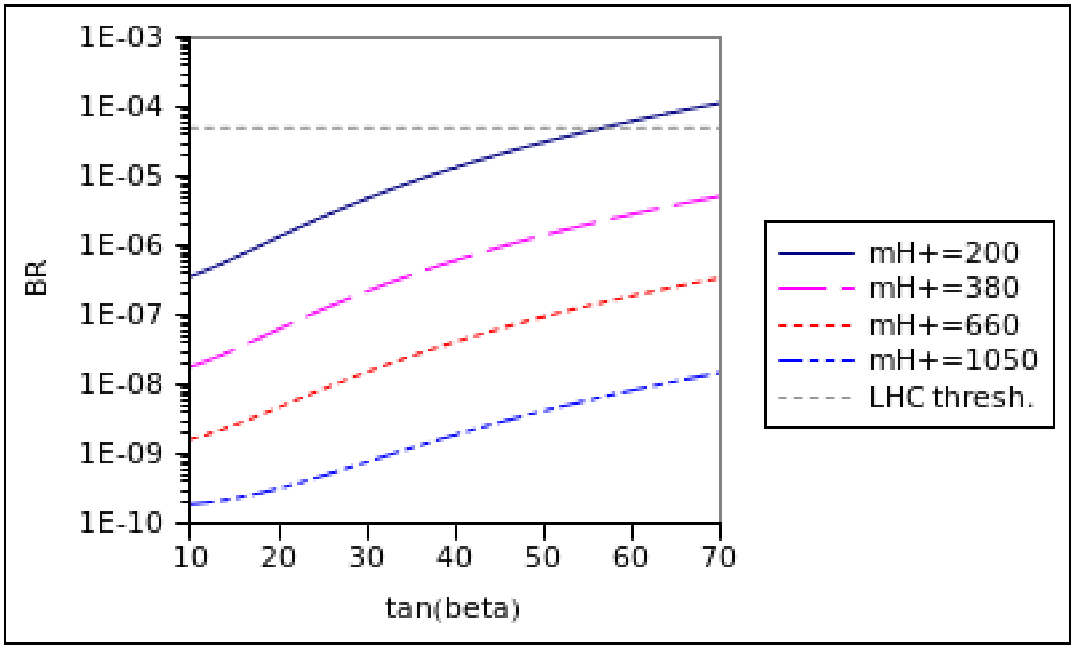

Figure 5.4: The $BR(t \rightarrow cH^0)$ as a function of $\tan\beta$ at various m_{H^+} in the T2HDM. We set m_{h^0} = 1000 GeV and m_{A^0} = 1200 GeV. "LHC thresh." stands for the limit of the LHC sensitivity at 100 fb^{-1}.

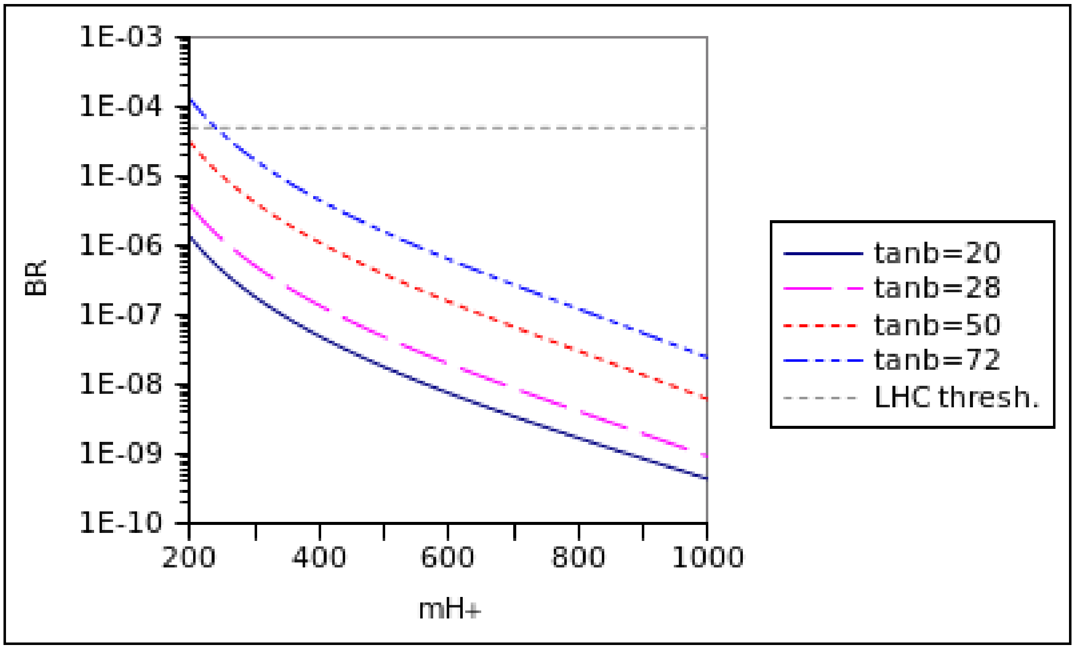

Figure 5.5: The $BR(t \rightarrow cH^0)$ as a function of m_{H^+} at various $\tan\beta$ in the T2HDM. We set m_{h^0} = 1000 GeV and m_{A^0} = 1200 GeV. "LHC thresh." stands for the limit of the LHC sensitivity at 100 fb^{-1}.

is a bit higher in the T2HDM than in the 2HDM-II. We note that the value $m_{H^+} = 200$ GeV is outside the 1σ bounds. We can see that, for a high m_{h^0}, the $BR\left(t \to cH^0\right)$ in the T2HDM is not as enhanced as expected relative to the 2HDM-II. We expected that the diagram with two charged scalar and a b quark will be enhanced in the T2HDM, since the $H^+\bar{c}b$ interaction is enhanced. We recall the Feynman rule for this interaction:

$$\frac{g}{\sqrt{2}m_W}\left[\tan\beta V_{cb} m_b R + m_c\left(-\tan\beta V_{cb} + \xi^*\left(\tan\beta + \cot\beta\right)V_{tb}\right)L\right], \tag{5.1}$$

and the amplitude of this diagram:

$$\begin{aligned} M_7 = \frac{-i\bar{u}_c}{16\pi^2} g^{3h}_{H^+H^+h}\Big[& m_b C_0\left(A^{H^+}_{cb} B^{H^+*}_{tb} L + B^{H^+}_{cb} A^{H^+*}_{tb} R\right) - m_c C_{12}\left(B^{H^+}_{cb} B^{H^+*}_{tb} L + A^{H^+}_{cb} A^{H^+*}_{tb} R\right) + \\ & + m_t\left(-C_{11} + C_{12}\right)\left(A^{H^+}_{cb} A^{H^+*}_{tb} L + B^{H^+}_{cb} B^{H^+*}_{tb} R\right)\Big] u_t, \end{aligned} \tag{5.2}$$

where C_{ij} are the Passarino-Veltman scalar functions (see App. D).

The term multiplied by the left projection operator is enhanced. In our notations it is denoted as $A^{H^+}_{cb}$ in (5.2). The leading term in the amplitude in the 2HDM-II, for $\tan\beta \gtrsim 10$, is $\propto m_t B^{H^+}_{cb} B^{H^+*}_{tb} \propto m_t m_b^2 \tan^2\beta V_{cb} V^*_{tb}$ (see Sec. 3). In the T2HDM this term does not receive a significant enhancement. However, the term $\propto m_b A^{H^+}_{cb} B^{H^+*}_{tb}$, which in the 2HDM-II is a sub-leading term, is in the T2HDM $\propto \xi^* m_c m_b^2 \tan^2\beta V_{tb} V^*_{tb}$, and is of the same order of magnitude as the leading term of the 2HDM-II (together with the C_{ij} loop functions). Thus we can summarize that what would have been a sub-leading term in the 2HDM-II, becomes in the T2HDM of the same order of magnitude of the leading term, and therefore the enhancement is not as significant as expected.

In the last two rows of the table we see the impact of the neutral Higgs sector, by setting a high m_{H^+}. The results are much higher in the T2HDM than in the 2HDM-II, which is to be expected, since the 2HDM-II does not have any tree-level FC interactions. However, the overall BR's in the small m_{h^0} regime are also small due to the cancellation of the leading term in the $h^0\bar{t}t$ vertex.

To complete the picture, we note that the SM value is only dependent upon the neutral Higgs mass. Setting $m_{H^0} = 91$ GeV, we get: $BR_{SM}\left(t \to cH^0\right) = 6.03 \times 10^{-14}$, for $m_{H^0} = 100$ GeV we get $BR_{SM}\left(t \to cH^0\right) = 4.63 \times 10^{-14}$, and for $m_{H^0} = 150$ GeV we get $BR_{SM}\left(t \to cH^0\right) = 5.26 \times 10^{-15}$.

5.2 Results for the 1-loop Higgs rare decay $H^0 \to \bar{t}c$

We recall the values that we use in the following plots, which were also given above: $m_{H^0} = 300$ GeV (chosen arbitrarily), $m_t = 172.5$ GeV, $m_c = 1.24$ GeV, $m_b = 4.20$ GeV, $m_W = 80.40$ GeV, $m_Z = 91.188$ GeV, $\alpha_{EW}\left(m_z\right) = 1/127.9$, and $\alpha = \beta$. The ξ and ξ' parameters are set to their best-fit value of Eq. (4.1): $|\xi| = 0.8$, $\varphi_\xi = 110°$, $|\xi'| = 0.21$, and $\varphi_{\xi'} = 250°$. The total Higgs width is calculated (see Sec. 4.4) from the decays $H^0 \to \bar{q}q$, $H^0 \to VV$, $H^0 \to h_i h_j$ and $H^0 \to V_i h_j$, as defined in App. E.

In Fig. 5.6 we present the SM value for the $BR\left(H^0 \to \bar{t}c + \bar{c}t\right)$. Our results agree with [4].

Next we turn to results in the T2HDM. In Fig. 5.7 we give a 3D plot of $BR\left(H^0 \to \bar{t}c + \bar{c}t\right)$ in the $m_{H^+} - \tan\beta$ plane in the T2HDM. We see the same tendency as in the decay $t \to cH^0$: The BR rises with $\tan\beta$ and rises with lower m_{H^+}.

In Figs. 5.8,5.9 we give 2D plots of the BR as a function of $\tan\beta$ and m_{H^+} respectively, with the same parameters as in Fig. 5.7. We see now more clearly the behavior described above.

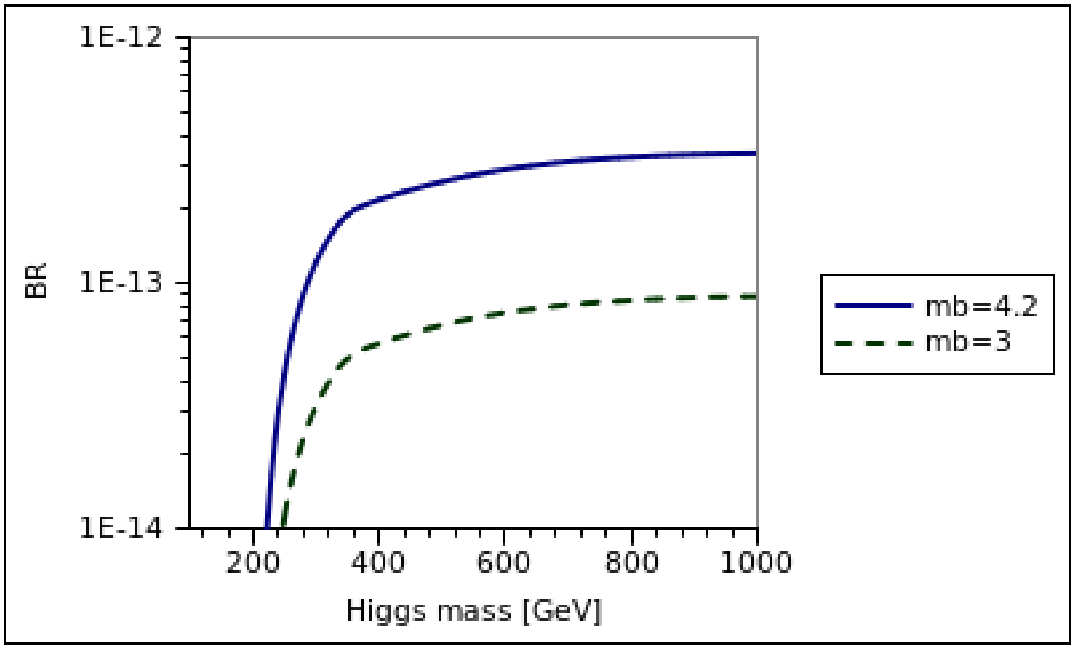

Figure 5.6: The SM value for the $BR(H^0 \to \bar{t}c + \bar{c}t)$ as a function of the Higgs mass, for $\overline{m_b}(\overline{m_b}) = 4.2$ GeV and for $\overline{m_b}(\overline{m_Z}) = 3$ GeV [27]. The BR is not sensitive to m_c.

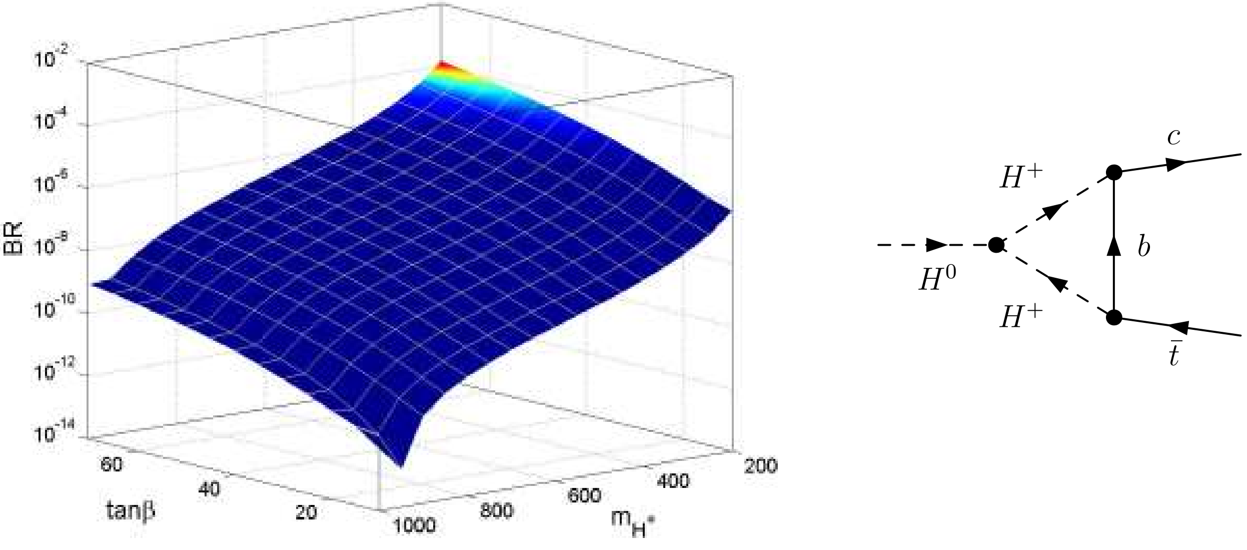

(a) (b)

Figure 5.7: (a) 3D plot of $BR(H^0 \to \bar{t}c + \bar{c}t)$ in the $m_{H^+} - \tan\beta$ plane in the T2HDM, and (b) the dominant diagram. We set $m_{h^0} = 1000$ GeV and $m_{A^0} = 1000$ GeV.

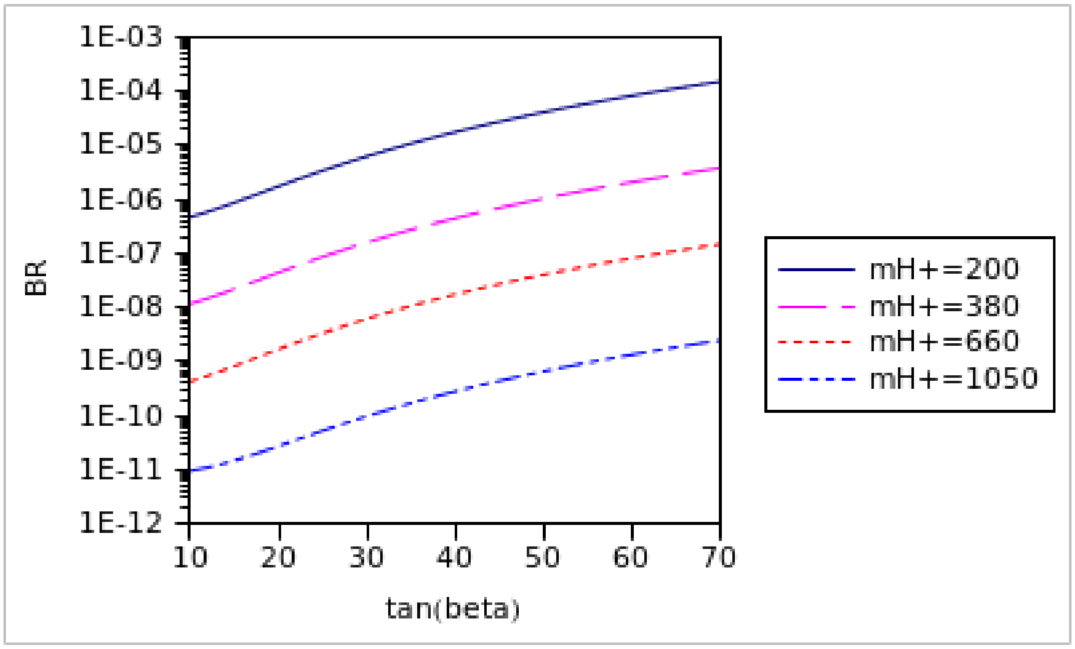

Figure 5.8: The $BR\,(H^0 \to \bar{t}c + \bar{c}t)$ as a function of $\tan\beta$ at different m_{H^+} in the T2HDM. We set $m_{h^0} = 1000$ GeV and $m_{A^0} = 1000$ GeV.

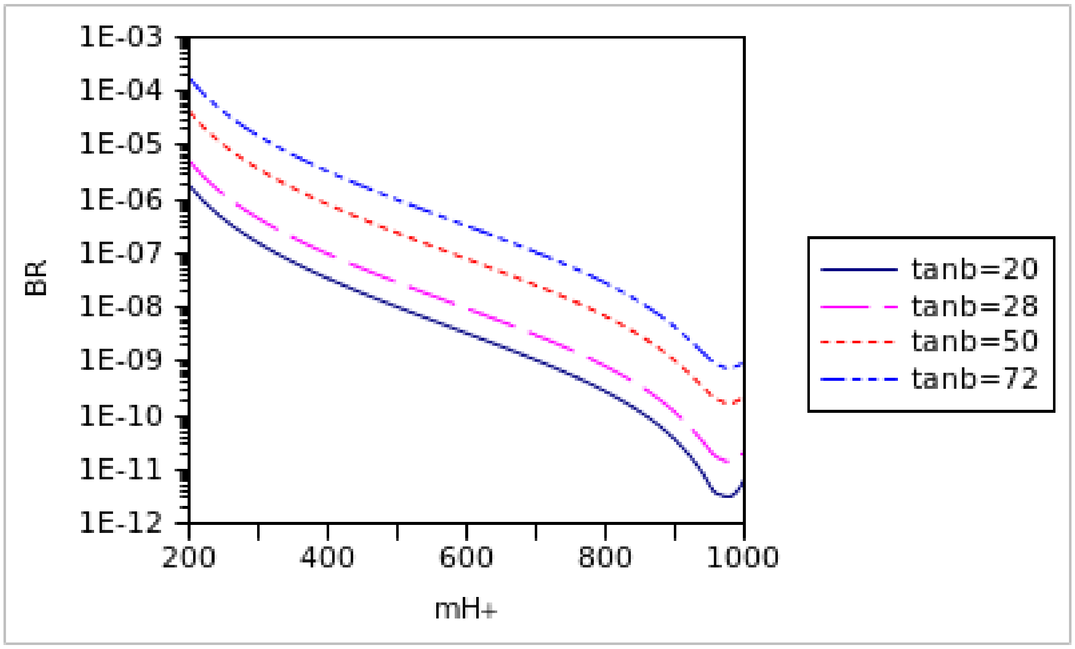

Figure 5.9: The $BR\,(H^0 \to \bar{t}c + \bar{c}t)$ as a function of m_{H^+} at different $\tan\beta$ in the T2HDM. We set $m_{h^0} = 1000$ GeV and $m_{A^0} = 1000$ GeV.

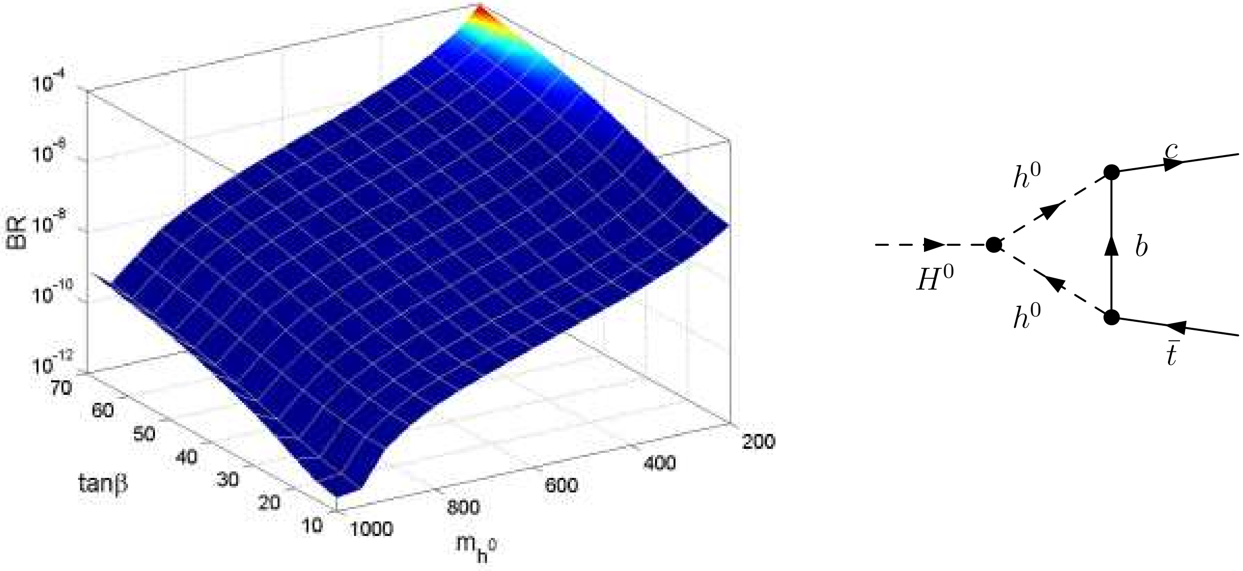

(a) (b)

Figure 5.10: (a) 3D plot of $BR\,(H^0 \to \bar{t}c + \bar{c}t)$ in the $m_{h^0} - \tan\beta$ plane in the T2HDM, and (b) the dominant diagram. We set $m_{H^+} = 1000$ GeV and $m_{A^0} = 1000$ GeV.

parameters	SM	2HDM-II	T2HDM
$m_{h^0} = 800$, $m_{A^0} = 1000$, $\tan\beta = 72$, $m_{H^+} = 200$	1.23×10^{-13}	1.26×10^{-4}	1.70×10^{-4}
$m_{h^0} = 800$, $m_{A^0} = 1000$, $\tan\beta = 72$, $m_{H^+} = 380$	1.23×10^{-13}	3.09×10^{-6}	4.45×10^{-6}
$m_{h^0} = 200$, $m_{A^0} = 4000$, $\tan\beta = 20$, $m_{H^+} = 1050$	1.23×10^{-13}	8.69×10^{-8}	2.90×10^{-4}
$m_{h^0} = 200$, $m_{A^0} = 1000$, $\tan\beta = 20$, $m_{H^+} = 1050$	1.23×10^{-13}	8.99×10^{-12}	9.11×10^{-7}

Table 5.2: Comparison of $BR\,(H^0 \to \bar{t}c + \bar{c}t)$ between the T2HDM, the 2HDM-II, and the SM. Masses are in units of GeV. We set $m_{H^0} = 300$, $\alpha = \beta$, and other parameters to their best-fit value of (4.1).

In Fig. 5.10 we give a 3D plot of $BR\,(H^0 \to \bar{t}c + \bar{c}t)$ in the $m_{h^0} - \tan\beta$ plane in the T2HDM, and in Fig. 5.11 we give a 2D plot of the BR as a function of $\tan\beta$ with the same parameters as Fig. 5.10 at several values of m_{h^0}. We can see that the BR rises with lower m_{h^0}, but has a weak dependence on $\tan\beta$.

In table 5.2 we give the $BR\,(H^0 \to \bar{t}c + \bar{c}t)$ values in the different models, for a few points in the parameter space. As can be seen, the behavior is similar to the $t \to cH^0$ process, although generally the BR values are higher.

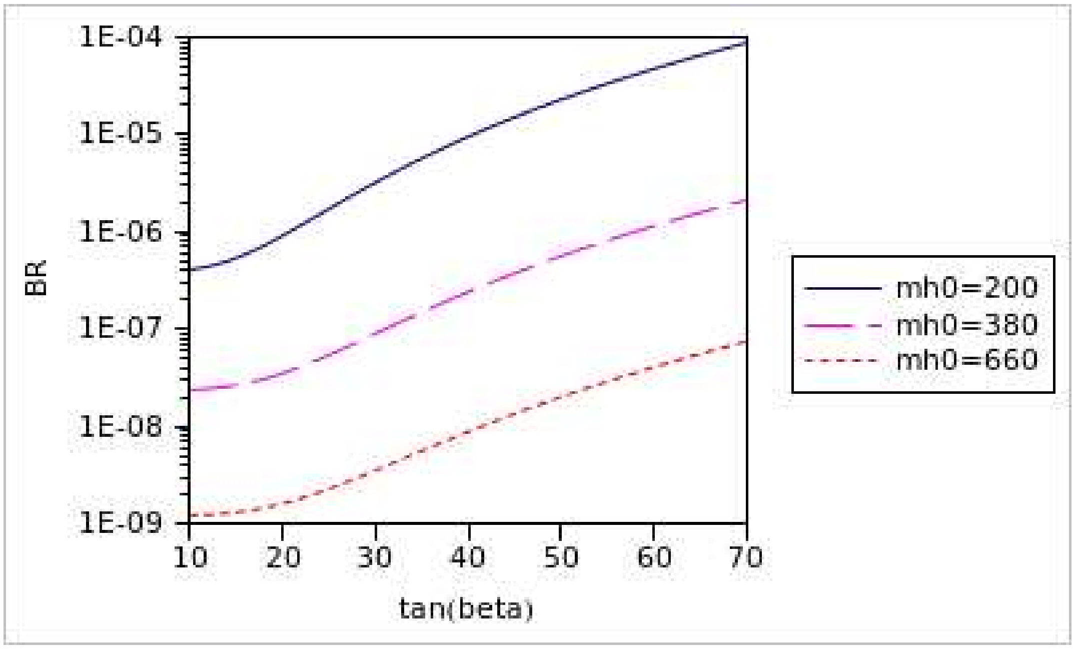

Figure 5.11: The $BR\,(H^0 \rightarrow \bar{t}c + \bar{c}t)$ as a function of $\tan\beta$ at different m_{h^0} in the T2HDM. We set $m_{H^+} = 1000$ GeV and $m_{A^0} = 1000$ GeV.

Chapter 6

Summary

The T2HDM is a distinct type of a 2HDM in which the top quark receives a special status. In this model, the top is coupled to the second Higgs doublet, while all other quarks are coupled to the first Higgs doublet. Assuming that the second Higgs VEV (v_2) is much larger than the first Higgs VEV (v_1), the top quark receives a much larger mass than all other quarks in a natural manner. Therefore the working assumption of the T2HDM is that $\tan\beta \equiv v_2/v_1 \gg 1$. In addition, these Yukawa couplings generate potentially enhanced flavor-changing (FC) interactions, both in the charged and the neutral sectors. These interactions can greatly enhance FC decays such as $t \to ch$ and $h \to \bar{t}c$.

The Yukawa sector of the model was explicitly (and independently) derived, as well as scalar self interactions. For example, the $H^+\bar{b}c$ vertex is enhanced by a factor of V_{tb}/V_{cb} compared to the corresponding 2HDM-II vertex. This enhancement motivated the present work, since it is expected to influence the 1-loop $t \to cH^0$ and $H^0 \to \bar{t}c$ decays via diagrams involving H^+ scalars and b quarks inside the loop.

In order to separate the 1-loop decays from the tree-level decays, we chose $\alpha = \beta$. This choice eliminates the $t \to cH^0$ and $H^0 \to \bar{t}c$ tree-level decays, so that these decays proceed at 1-loop. On the other hand, the decays $t \to ch^0$ and $h^0 \to \bar{t}c$ occur at the tree-level for $\alpha = \beta$. For these tree-level decays we gave explicit formulae. The $h^0\bar{t}c$ neutral FC interaction can also enhance the 1-loop $BR\,(t \to cH^0)$ and $BR\,(H^0 \to \bar{t}c)$, via diagrams involving h^0 scalars and t quarks inside the loop.

The parameter space of the T2HDM was explored for the resulting 1-loop $BR\,(t \to cH^0)$ and $BR\,(H^0 \to \bar{t}c)$. We focused on those regions of the parameter space in which these BR's can be much higher than in the SM and 2HDM-I,II. We found the dynamics of the two processes to be similar, which was expected since their amplitudes and rates are related by crossing symmetry. The 1-loop $BR\,(t \to cH^0)$ can reach $\sim 10^{-4}$ in the T2HDM. This is above the LHC detection threshold of 5×10^{-5}, and above the SM, and 2HDM-I,II predictions. The 1-loop $BR\,(H^0 \to \bar{t}c)$ can reach above $\sim 10^{-4}$ in the T2HDM, higher than the SM and 2HDM-I,II predictions.

We conclude that if such decays are indeed identified at the LHC, then the dynamics of the T2HDM type will be especially motivated.

Appendix A

Higgs potential in two Higgs doublet models

In the following we introduce the Higgs potential of a general 2HDM, which corresponds to the T2HDM as well as to 2HDM's of types I, II and III.
We assume a CP conserving Higgs potential of the form [5]:

$$\begin{aligned}\mathcal{L}_H &= \lambda_1\left(\Phi_1^\dagger\Phi_1 - v_1^2/2\right)^2 + \lambda_2\left(\Phi_2^\dagger\Phi_2 - v_2^2/2\right)^2 + \lambda_3\left[\left(\Phi_1^\dagger\Phi_1 - v_1^2/2\right) + \left(\Phi_2^\dagger\Phi_2 - v_2^2/2\right)\right]^2 + \\ &\quad +\lambda_4\left[\left(\Phi_1^\dagger\Phi_1\right)\left(\Phi_2^\dagger\Phi_2\right) - \left(\Phi_1^\dagger\Phi_2\right)\left(\Phi_2^\dagger\Phi_1\right)\right] + \lambda_5\left|\Phi_1^\dagger\Phi_2 - v_1v_2/2\right|^2, \qquad (A.1)\end{aligned}$$

already introduced in Sec. 2, and:

$$\Phi_{1,2} = \begin{pmatrix} \Phi^+_{1,2} \\ \frac{v_{1,2}+\Phi^{0r}_{1,2}+i\Phi^{0i}_{1,2}}{\sqrt{2}} \end{pmatrix}. \qquad (A.2)$$

This potential has five couplings λ_i plus two VEV's v_1 and v_2, seven degrees of freedom in total. These will be later expressed in terms of 5 masses of the physical scalars, plus two angles. We will then extract the Feynman rules of the 3-scalar interactions, expressing them in terms of the physical masses and angles.
We assume a potential which conserves CP. The absence of CP violation implies that the CP-even h^0, H^0 and the CP-odd A^0, G^0 mix separately, as we will later see. CP violation in the scalar potential would mix CP-even and odd scalars (H^0, h^0, A^0), as discussed in [5].
The wearying part is deriving the Feynman rules in terms of the masses and angles instead of λ_i ,v_1 and v_2. The explicit derivation is straightforward and we will not follow it completely here. We will, however, introduce the important formulae, following the notation of [5].
The fields can always be redefined so that their VEV's are real, without affecting the potential.
The VEV's as defined can be easily seen to minimize the potential.
The mass terms of the neutral real (CP-even) scalars can be combined into a symmetric bilinear mass term:

$$\begin{aligned}\mathcal{L}_{m-CPE} &= \left(\Phi_1^{0r}, \Phi_2^{0r}\right)\frac{1}{2}\left[\frac{1}{2}\begin{pmatrix} 4v_1^2\left(\lambda_1+\lambda_3\right)+v_2^2\lambda_5 & \left(4\lambda_3+\lambda_5\right)v_1v_2 \\ \left(4\lambda_3+\lambda_5\right)v_1v_2 & 4v_2^2\left(\lambda_2+\lambda_3\right)+v_1^2\lambda_5 \end{pmatrix}\right]\begin{pmatrix}\Phi_1^{0r}\\ \Phi_2^{0r}\end{pmatrix} \equiv \\ &\equiv \frac{1}{2}\left(\Phi^{0r}\right)^T[M]\left(\Phi^{0r}\right). \qquad (A.3)\end{aligned}$$

The mass-squared matrix, M, can be diagonalized using the rotation matrix $\begin{bmatrix}\cos\alpha & -\sin\alpha \\ \sin\alpha & \cos\alpha\end{bmatrix}$, with an angle α such that:

$$\sin 2\alpha = \frac{2M_{12}}{\sqrt{(M_{11}-M_{22})^2+4M_{12}^2}} \quad , \qquad \cos 2\alpha = \frac{M_{11}-M_{22}}{\sqrt{(M_{11}-M_{22})^2+4M_{12}^2}}, \tag{A.4}$$

which defines the CP-even neutral scalars in the mass basis:

$$\begin{aligned} H^0 &= \Phi_1^{or}\cos\alpha + \Phi_2^{or}\sin\alpha, \\ h^0 &= -\Phi_1^{or}\sin\alpha + \Phi_2^{or}\cos\alpha, \end{aligned} \tag{A.5}$$

with masses:

$$m^2_{H^0,h^0} = \frac{1}{2}(M_{11}+M_{22}) \pm \frac{1}{2}\sqrt{(M_{11}-M_{22})^2+4M_{12}^2} \ . \tag{A.6}$$

The CP-odd neutral scalars have a simpler mass^2 matrix: $\lambda_5 \left[\frac{1}{2}\begin{pmatrix} v_2^2 & -v_1v_2 \\ -v_1v_2 & v_1^2 \end{pmatrix}\right]$ diagonalized using the rotation matrix with the angle β such that:

$$\tan\beta = \frac{v_2}{v_1} \ , \tag{A.7}$$

which defines the CP-odd neutral scalars and unphysical Goldstone boson (G^0), in the mass basis:

$$\begin{aligned} G^0 &= \Phi_1^{oi}\cos\beta + \Phi_2^{oi}\sin\beta, \\ A^0 &= -\Phi_1^{oi}\sin\beta + \Phi_2^{oi}\cos\beta, \end{aligned} \tag{A.8}$$

with mass: $m^2_{A^0} = \lambda_5 v^2/2$ (recall that: $v = \sqrt{v_1^2+v_2^2} = \frac{2m_W}{g}$).
We can see that the CP-even h^0, H^0 and the CP-odd A^0, G^0 mix separately, as promised.
The charged scalars have a similar mass^2 matrix: $\lambda_4 \left[\frac{1}{2}\begin{pmatrix} v_2^2 & -v_1v_2 \\ -v_1v_2 & v_1^2 \end{pmatrix}\right]$, diagonalized with the same angle β, defining the charged physical scalars and unphysical Goldstone bosons ($G^\pm$), in the mass basis:

$$\begin{aligned} G^\pm &= \Phi_1^\pm\cos\beta + \Phi_2^\pm\sin\beta, \\ H^\pm &= -\Phi_1^\pm\sin\beta + \Phi_2^\pm\cos\beta, \end{aligned} \tag{A.9}$$

with mass: $m^2_{H^\pm} = \lambda_4 v^2/2$.
As we stated above, we want to express the triple-scalar couplings in terms of masses and angles instead of λ_i, v_j. We will first connect between M_{ij} and λ_i, v_j:

$$\begin{pmatrix} M_{11} \\ M_{22} \\ M_{12} \end{pmatrix} = \begin{bmatrix} 4v_1^2 & 0 & 4v_1^2 \\ 0 & 4v_2^2 & 4v_2^2 \\ 0 & 0 & 4v_1v_2 \end{bmatrix} \begin{pmatrix} \lambda_1 \\ \lambda_2 \\ \lambda_3 \end{pmatrix} + \begin{pmatrix} v_2^2\lambda_5 \\ v_1^2\lambda_5 \\ v_1v_2\lambda_5 \end{pmatrix} . \tag{A.10}$$

We can invert the equation, and insert $\lambda_5 = \frac{m^2_{A^0}}{v^2}$, to write:

$$\begin{aligned}\lambda_1+\lambda_3 &= \frac{1}{4}\left(\frac{M_{11}}{v_1^2}-\tan^2\beta\frac{m_{A^0}^2}{v^2}\right),\\ \lambda_2+\lambda_3 &= \frac{1}{4}\left(\frac{M_{22}}{v_2^2}-\cot^2\beta\frac{m_{A^0}^2}{v^2}\right),\\ \lambda_3+\frac{1}{2}\lambda_5 &= \frac{1}{4}\left(\frac{M_{12}}{v_1v_2}+\frac{m_{A^0}^2}{v^2}\right).\end{aligned}\tag{A.11}$$

The neutral CP-even couplings can be collected from (A.1):

$$\begin{aligned}\mathcal{L}_{3h}^{CP-even} &= 4v_1\left(\Phi_1^{0r}\right)^3(\lambda_1+\lambda_3)+4v_2\left(\Phi_2^{0r}\right)^3(\lambda_2+\lambda_3)+\\ &\quad +4v_1\Phi_1^{0r}\left(\Phi_2^{0r}\right)^2\left(\lambda_3+\frac{1}{2}\lambda_5\right)+4v_2\Phi_2^{0r}\left(\Phi_1^{0r}\right)^2\left(\lambda_3+\frac{1}{2}\lambda_5\right)=\\ &= v_1\left(H_0\cos\alpha-h_0\sin\alpha\right)^3\left(\frac{M_{11}}{v_1^2}-\tan^2\beta\frac{m_{A^0}^2}{v^2}\right)+\\ &\quad +v_2\left(H_0\sin\alpha+h_0\cos\alpha\right)^3\left(\frac{M_{22}}{v_2^2}-\cot^2\beta\frac{m_{A^0}^2}{v^2}\right)+\\ &\quad +v_1\left(H_0\cos\alpha-h_0\sin\alpha\right)\left(H_0\sin\alpha+h_0\cos\alpha\right)^2\left(\frac{M_{12}}{v_1v_2}+\frac{m_{A^0}^2}{v^2}\right)+\\ &\quad +v_2\left(H_0\sin\alpha+h_0\cos\alpha\right)\left(H_0\cos\alpha-h_0\sin\alpha\right)^2\left(\frac{M_{12}}{v_1v_2}+\frac{m_{A^0}^2}{v^2}\right).\end{aligned}\tag{A.12}$$

For example, focusing on the $h^0h^0H^0$ term, and using $v_1=v\cos\beta$, $v_2=v\sin\beta$, we get:

$$\begin{aligned}\mathcal{L}_{h^0h^0H^0} &= \frac{1}{v}\left\{3\cos\beta\cos\alpha\sin^2\alpha\left(\frac{M_{11}}{\cos^2\beta}-\tan^2\beta m_{A^0}^2\right)+3\sin\beta\sin\alpha\cos^2\alpha\left(\frac{M_{22}}{\sin^2\beta}-\cot^2\beta m_{A^0}^2\right)+\right.\\ &\quad \left.+\left[\cos(\alpha+\beta)\cos2\alpha-\sin(\alpha+\beta)\sin\alpha\cos\alpha\right]\left(\frac{M_{12}}{\cos\beta\sin\beta}+m_{A^0}^2\right)\right\}.\end{aligned}\tag{A.13}$$

In order to arrive to the final form, more algebraic work is needed. Using (A.4), from which follows also: $2M_{12}\cos2\alpha=(M_{11}-M_{22})\sin2\alpha$, and (A.6), from which follows also $M_{11}+M_{22}=m_{h^0}^2+m_{H^0}^2$, and other trigonometric identities, we arrive at:

$$\mathcal{L}_{h^0h^0H^0} = \frac{g\cos(\beta-\alpha)}{2m_W\sin2\beta}\left[\sin2\alpha\left(2m_{h^0}^2+m_{H^0}^2\right)-m_{A^0}^2\left(3\sin2\alpha-\sin2\beta\right)\right],\tag{A.14}$$

which agrees with [15], and which is expressed in terms of the physical masses and mixing angles.

All other 3-scalar interactions are derived similarly. In App. (B) we listed all the vertices relevant to the present work.

We note that we did not find the $h^0H^0H^0$ coupling for the higgs potential of (A.1) in the literature and it was therefore derived by us.

Appendix B

Feynman rules for two Higgs doublet models

In this section we list the Feynman rules for the 2HDM's that were used in this work, in the t'Hooft Feynman gauge. The Feynman rules are presented in Fig. B.1.
In table B.1 we give the Yukawa Feynman rules of the T2HDM and of the 2HDM type II. The other Feynman rules are common to all 2HDM's.
In table B.2 we give the vector-vector-scalar couplings, common to all 2HDM's, from [5].
In table B.3 we give the vector-scalar-scalar couplings, we define the vertices as in [5], where the second particle is outgoing.
The vertices $Z^0G^0H^0$, $Z^0G^0h^0$ do not participate in the calculations since the corresponding Yukawa vertex $\bar{q}qG^0$ does not generate FC interactions.
Now we turn to the 3-scalar interactions. We were not able to find all vertices in the literature, and therefore we derived one vertex ($h^0H^0H^0$), while the rest of the scalar self interactions can be found in [15]. We give in table B.4 the complete list of the 3-scalar interactions that were used in this work.

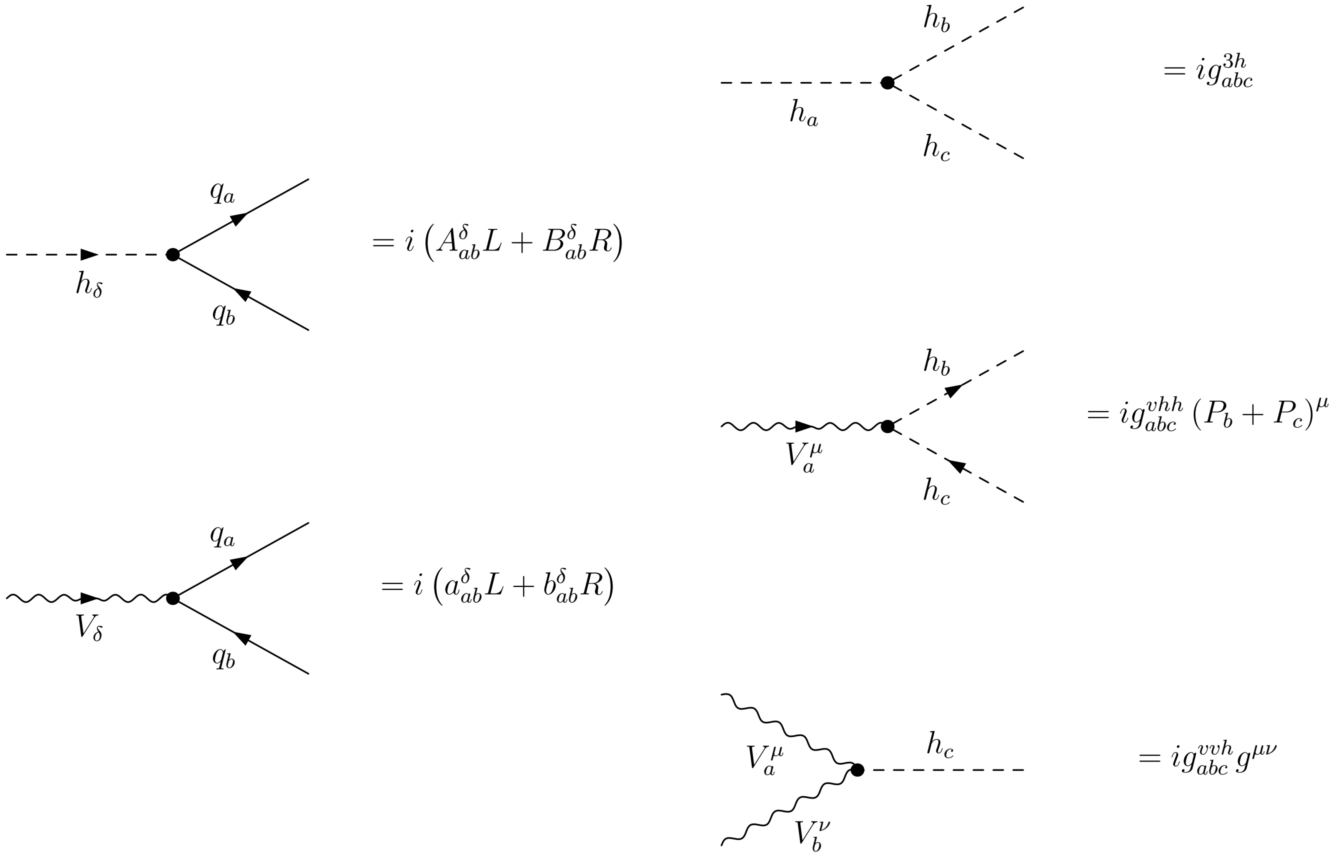
h_b
h_a
h_c
$= ig^{3h}_{abc}$
q_a
h_δ
q_b
$= i\left(A^\delta_{ab}L + B^\delta_{ab}R\right)$
h_b
V^μ_a
h_c
$= ig^{vhh}_{abc}\,(P_b + P_c)^\mu$
q_a
V_δ
q_b
$= i\left(a^\delta_{ab}L + b^\delta_{ab}R\right)$
V^μ_a
h_c
V^ν_b
$= ig^{vvh}_{abc}\,g^{\mu\nu}$

Figure B.1: Feynman rules.

	T2HDM	2HDM-II [5]
$H^0\bar{u}_j u_i$	$\frac{g}{2m_W}\left(-M_u\frac{\cos\alpha}{\cos\beta} + \Sigma\left(-\frac{\sin\alpha}{\sin\beta} + \frac{\cos\alpha}{\cos\beta}\right)\right)R + (h.c.)\,L$	$-\frac{gM_u}{2m_W}\frac{\sin\alpha}{\sin\beta}$
$h^0\bar{u}u$	$\frac{g}{2m_W}\left(M_u\frac{\sin\alpha}{\cos\beta} - \Sigma\left(\frac{\cos\alpha}{\sin\beta} + \frac{\sin\alpha}{\cos\beta}\right)\right)R + (h.c.)\,L$	$-\frac{gM_u}{2m_W}\frac{\cos\alpha}{\sin\beta}$
$A^0\bar{u}u$	$i\frac{g}{2m_W}\left(-M_u\tan\beta + \Sigma\left(\tan\beta + \cot\beta\right)\right)R + (h.c.)\,L$	$i\frac{gM_u}{2m_W}\cot\beta\,(R - L)$
$G^0\bar{u}u$	$i\frac{gM_u}{2m_W}\,(R - L)$	$i\frac{gM_u}{2m_W}\,(R - L)$
$H^0\bar{d}d$	$-\frac{gM_d}{2m_W}\frac{\cos\alpha}{\cos\beta}$	$-\frac{gM_d}{2m_W}\frac{\cos\alpha}{\cos\beta}$
$h^0\bar{d}d$	$\frac{gM_d}{2m_W}\frac{\sin\alpha}{\cos\beta}$	$\frac{gM_d}{2m_W}\frac{\sin\alpha}{\cos\beta}$
$A^0\bar{d}d$	$i\frac{gM_d}{2m_W}\tan\beta\,(R - L)$	$i\frac{gM_d}{2m_W}\tan\beta\,(R - L)$
$G^0\bar{d}d$	$-i\frac{gM_d}{2m_W}\,(R - L)$	$-i\frac{gM_d}{2m_W}\,(R - L)$
$H^+\bar{u}d$	$\frac{g}{\sqrt{2}m_W}\left[\tan\beta V_{CKM}M_dR + \left(-M_u\tan\beta + \Sigma\left(\tan\beta + \cot\beta\right)\right)V_{CKM}L\right]$	$\frac{g}{\sqrt{2}m_W}\left[\tan\beta V_{CKM}M_dR + \cot\beta M_uV_{CKM}L\right]$
$G^+\bar{u}d$	$\frac{g}{\sqrt{2}m_W}\left(M_uV_{CKM}L - V_{CKM}M_dR\right)$	$\frac{g}{\sqrt{2}m_W}\left(M_uV_{CKM}L - V_{CKM}M_dR\right)$

Table B.1: Feynman rules for Yukawa interactions in the T2HDM and in the 2HDM-II.

$W^+W^-H^0$	$igm_W \cos(\beta-\alpha)\, g^{\mu\nu}$
$W^+W^-h^0$	$igm_W \sin(\beta-\alpha)\, g^{\mu\nu}$
$Z^0Z^0H^0$	$\frac{igm_Z}{\cos\theta_W} \cos(\beta-\alpha)\, g^{\mu\nu}$
$Z^0Z^0h^0$	$\frac{igm_Z}{\cos\theta_W} \sin(\beta-\alpha)\, g^{\mu\nu}$

Table B.2: Feynman rules for vector-vector-scalar interactions [5].

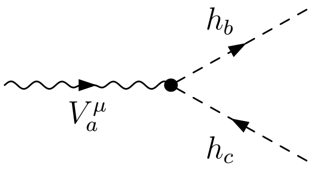	$= ig^{vhh}_{abc}\,(P_b + P_c)^\mu$
$W^+H^+H^0$	$i\frac{g}{2}\sin(\beta-\alpha)\,(P_{H^+} + P_{H^0})^\mu$
$W^+H^+h^0$	$-i\frac{g}{2}\cos(\beta-\alpha)\,(P_{H^+} + P_{h^0})^\mu$
$W^+G^+H^0$	$-i\frac{g}{2}\cos(\beta-\alpha)\,(P_{G^+} + P_{H^0})^\mu$
$W^+G^+h^0$	$-i\frac{g}{2}\sin(\beta-\alpha)\,(P_{G^+} + P_{h^0})^\mu$
$Z^0A^0H^0$	$-\frac{g\sin(\beta-\alpha)}{2\cos\theta_W}\,(P_{A^0} + P_{H^0})^\mu$
$Z^0A^0h^0$	$\frac{g\cos(\beta-\alpha)}{2\cos\theta_W}\,(P_{A^0} + P_{h^0})^\mu$

Table B.3: Feynman rules for vector-scalar-scalar interactions [5].

$H^+H^-H^0$	$-\frac{g}{m_W}\left[\left(m^2_{H^+} - m^2_{A^0} + \frac{1}{2}m^2_{H^0}\right)\cos(\beta-\alpha) + \left(m^2_{A^0} - m^2_{H^0}\right)\cot 2\beta \sin(\beta-\alpha)\right]$
$H^+H^-h^0$	$-\frac{g}{m_W}\left[\left(m^2_{H^+} - m^2_{A^0} + \frac{1}{2}m^2_{h^0}\right)\sin(\beta-\alpha) + \left(m^2_{h^0} - m^2_{A^0}\right)\cot 2\beta \cos(\beta-\alpha)\right]$
$h^0h^0H^0$	$-\frac{g\cos(\beta-\alpha)}{2m_W\sin 2\beta}\left[\left(2m^2_{h^0} + m^2_{H^0}\right)\sin 2\alpha - m^2_{A^0}\left(3\sin 2\alpha - \sin 2\beta\right)\right]$
$h^0H^0H^0$	$-\frac{g\sin(\beta-\alpha)}{2m_W\sin 2\beta}\left[\left(2m^2_{H^0} + m^2_{h^0}\right)\sin 2\alpha - m^2_{A^0}\left(3\sin 2\alpha + \sin 2\beta\right)\right]$
$A^0A^0H^0$	$-\frac{g}{2m_W}\left[m^2_{H^0}\cos(\beta-\alpha) + 2\left(m^2_{H^0} - m^2_{A^0}\right)\cot 2\beta \sin(\beta-\alpha)\right]$
$A^0A^0h^0$	$-\frac{g}{2m_W}\left[m^2_{h^0}\sin(\beta-\alpha) + 2\left(m^2_{h^0} - m^2_{A^0}\right)\cot 2\beta \cos(\beta-\alpha)\right]$
$H^+G^-H^0$	$-i\frac{g}{2m_W}\left(m^2_{H^+} - m^2_{H^0}\right)\sin(\beta-\alpha)$
$H^+G^-h^0$	$i\frac{g}{2m_W}\left(m^2_{H^+} - m^2_{h^0}\right)\cos(\beta-\alpha)$
$G^+G^-H^0$	$-i\frac{g}{2m_W}m^2_{H^0}\cos(\beta-\alpha)$
$G^+G^-h^0$	$-i\frac{g}{2m_W}m^2_{h^0}\sin(\beta-\alpha)$

Table B.4: Feynman rules for triple-scalar interactions [15, 5].

Appendix C

1-loop diagrams calculation

In this appendix we give the 1-loop calculation of the 10 diagrams shown in Fig. 4.1. The calculation was done in the t'Hooft Feynman gauge.

In the t'Hooft Feynman gauge the vector bosons propagators reduce to their simplest form: $\Delta = ig^{\mu\nu}\left[p^2 - m^2 + i\epsilon\right]^{-1}$, and the Goldstone bosons mass is set equal to the respective gauge bosons: $m_{G^+} = m_{W^+}$, $m_{G^0} = m_Z$. The t'Hooft Feynman gauge was chosen because the calculation of each diagram is simpler.

definitions:

M_n – the amplitude corresponding to diagram n

h – the external neutral scalar

i – ($= t$) when used as index, the incoming fermion - the top

j – ($= c$) when used as index, the outgoing fermion - the charm

α, β – when used as indices, internal bosons (vectors or scalars) in the loop

l, k, q – when used as indices, internal fermions

L, R – the Left,Right projection operators

$\bar{u}_j$ – ($= \bar{u}(P_j)$) the outgoing spinor of the charm

u_i – ($= u(P_i)$) the incoming spinor of the top

B_0, B_1, C_0, C_{ij} – the n-point integral functions, defined in App. D

$A^{\delta}_{ab}, B^{\delta}_{ab}$ – the left,right -handed parts of the fermion-fermion-scalar vertex

$a^{\delta}_{ab}, b^{\delta}_{ab}$ – the left,right -handed parts of the fermion-fermion-vector vertex, for both charged and neutral gauge bosons

$g^{3h,vhh,vvh}_{abc}$ – the vertex of 3-scalars, vector-scalar-scalar, vector-vector-scalar, respectively

$g^{\mu\nu}$ – the metric, $g^{\mu\nu} = diag(1, -1, -1, -1)$

$$
\begin{aligned}
M_1 = \frac{i\bar{u}_j}{16\pi^2}\frac{-1}{m_i^2-m_l^2}&\left[m_l m_k B_0\left(B_{lj}^{h*}A_{lk}^{\alpha}B_{ik}^{\alpha*}L + A_{lj}^{h*}B_{lk}^{\alpha}A_{ik}^{\alpha*}R\right) +\right.\\
&- m_l m_i B_1\left(B_{lj}^{h*}A_{lk}^{\alpha}A_{ik}^{\alpha*}L + A_{lj}^{h*}B_{lk}^{\alpha}B_{ik}^{\alpha*}R\right) + m_i m_k B_0\left(B_{lj}^{h*}B_{lk}^{\alpha}A_{ik}^{\alpha*}L + A_{lj}^{h*}A_{lk}^{\alpha}B_{ik}^{\alpha*}R\right) +\\
&\left.-m_i^2 B_1\left(B_{lj}^{h*}B_{lk}^{\alpha}B_{ik}^{\alpha*}L + A_{lj}^{h*}A_{lk}^{\alpha}A_{ik}^{\alpha*}R\right)\right]u_i,
\end{aligned}
\tag{C.1}
$$

where $B = B\left(m_k^2, m_\alpha^2, m_i^2\right)$.

$$
\begin{aligned}
M_2 = \frac{i\bar{u}_j}{16\pi^2}\frac{-1}{m_j^2-m_l^2}&\left[m_l m_k B_0\left(A_{jk}^{\alpha}B_{lk}^{\alpha*}B_{il}^{h*}L + B_{jk}^{\alpha}A_{lk}^{\alpha*}A_{il}^{h*}R\right) +\right.\\
&+ m_k m_j B_0\left(B_{jk}^{\alpha}A_{lk}^{\alpha*}B_{il}^{h*}L + A_{jk}^{\alpha}B_{lk}^{\alpha*}A_{il}^{h*}R\right) - m_j m_l B_1\left(B_{jk}^{\alpha}B_{lk}^{\alpha*}B_{il}^{h*}L + A_{jk}^{\alpha}A_{lk}^{\alpha*}A_{il}^{h*}R\right) +\\
&\left.-m_j^2 B_1\left(A_{jk}^{\alpha}A_{lk}^{\alpha*}B_{il}^{h*}L + B_{jk}^{\alpha}B_{lk}^{\alpha*}A_{il}^{h*}R\right)\right]u_i,
\end{aligned}
\tag{C.2}
$$

where $B = B\left(m_k^2, m_\alpha^2, m_j^2\right)$.

$$
\begin{aligned}
M_3 = \frac{i\bar{u}_j}{16\pi^2}\frac{1}{m_i^2-m_l^2}&\left[4m_l m_k B_0\left(B_{lj}^{h*}b_{lk}^{\alpha}a_{ik}^{\alpha*}L + A_{lj}^{h*}a_{lk}^{\alpha}b_{ik}^{\alpha*}R\right) +\right.\\
&+ 2m_l m_i B_1\left(B_{lj}^{h*}b_{lk}^{\alpha}b_{ik}^{\alpha*}L + A_{lj}^{h*}a_{lk}^{\alpha}a_{ik}^{\alpha*}R\right) + 4m_i m_k B_0\left(B_{lj}^{h*}a_{lk}^{\alpha}b_{ik}^{\alpha*}L + A_{lj}^{h*}b_{lk}^{\alpha}a_{ik}^{\alpha*}R\right) +\\
&\left.+2m_i^2 B_1\left(B_{lj}^{h*}a_{lk}^{\alpha}a_{ik}^{\alpha*}L + A_{lj}^{h*}b_{lk}^{\alpha}b_{ik}^{\alpha*}R\right)\right]u_i,
\end{aligned}
\tag{C.3}
$$

where $B = B\left(m_k^2, m_\alpha^2, m_i^2\right)$.

$$
\begin{aligned}
M_4 = \frac{i\bar{u}_j}{16\pi^2}\frac{1}{m_j^2-m_l^2}&\left[4m_l m_k B_0\left(b_{jk}^{\alpha}a_{lk}^{\alpha*}B_{il}^{h*}L + a_{jk}^{\alpha}b_{lk}^{\alpha*}A_{il}^{h*}R\right) +\right.\\
&+ 4m_k m_j B_0\left(a_{jk}^{\alpha}b_{lk}^{\alpha*}B_{il}^{h*}L + b_{jk}^{\alpha}a_{lk}^{\alpha*}A_{il}^{h*}R\right) + 2m_j m_l B_1\left(a_{jk}^{\alpha}a_{lk}^{\alpha*}B_{il}^{h*}L + b_{jk}^{\alpha}b_{lk}^{\alpha*}A_{il}^{h*}R\right) +\\
&\left.+2m_j^2 B_1\left(b_{jk}^{\alpha}b_{lk}^{\alpha*}B_{il}^{h*}L + a_{jk}^{\alpha}a_{lk}^{\alpha*}A_{il}^{h*}R\right)\right]u_i,
\end{aligned}
\tag{C.4}
$$

where $B = B\left(m_k^2, m_\alpha^2, m_j^2\right)$.

$$
\begin{aligned}
M_5 = \frac{-i\bar{u}_j}{16\pi^2}&\left(A_{jq}^{\alpha}L + B_{jq}^{\alpha}R\right)\left\{\left[\tilde{C}_0 + m_i^2 C_{11} + \left(m_h^2 - m_i^2\right)C_{12}\right]\left(A_{jq}^{\alpha}A_{kq}^{h*}B_{ik}^{\alpha*}L + B_{jq}^{\alpha}B_{kq}^{h*}A_{ik}^{\alpha*}R\right) +\right.\\
&- m_q m_i C_{11}\left(A_{jq}^{\alpha}B_{kq}^{h*}A_{ik}^{\alpha*}L + B_{jq}^{\alpha}A_{kq}^{h*}B_{ik}^{\alpha*}R\right) + m_q m_j C_{12}\left(B_{jq}^{\alpha}A_{kq}^{h*}B_{ik}^{\alpha*}L + A_{jq}^{\alpha}B_{kq}^{h*}A_{ik}^{\alpha*}R\right) +\\
&+ m_i m_j\left(C_{12} - C_{11}\right)\left(B_{jq}^{\alpha}B_{kq}^{h*}A_{ik}^{\alpha*}L + A_{jq}^{\alpha}A_{kq}^{h*}B_{ik}^{\alpha*}R\right) + m_q m_k C_0\left(A_{jq}^{\alpha}B_{kq}^{h*}B_{ik}^{\alpha*}L + B_{jq}^{\alpha}A_{kq}^{h*}A_{ik}^{\alpha*}R\right) +\\
&- m_i m_k\left(C_{11} + C_0\right)\left(A_{jq}^{\alpha}A_{kq}^{h*}A_{ik}^{\alpha*}L + B_{jq}^{\alpha}B_{kq}^{h*}B_{ik}^{\alpha*}R\right) +\\
&\left.+m_j m_k\left(C_{12} + C_0\right)\left(B_{jq}^{\alpha}B_{kq}^{h*}B_{ik}^{\alpha*}L + A_{jq}^{\alpha}A_{kq}^{h*}A_{ik}^{\alpha*}R\right)\right\}u_i,
\end{aligned}
\tag{C.5}
$$

where $C = C\left(m_k^2, m_\alpha^2, m_q^2, m_i^2, m_j^2, m_h^2\right)$.

$$\begin{aligned} M_6 = \frac{i\bar{u}_j}{16\pi^2} \Big\{ & \Big[4\tilde{C}_0 + 2\left(m_i^2 - m_j^2 + m_h^2\right) C_{11} + 2\left(-m_i^2 + m_j^2 + m_h^2\right) C_{12} \Big] \left(b_{jq}^{\alpha} B_{kq}^{h*} a_{ik}^{\alpha*} L + a_{jq}^{\alpha} A_{kq}^{h*} b_{ik}^{\alpha*} R \right) + \\ & + 2m_q m_i C_{11} \left(b_{jq}^{\alpha} A_{kq}^{h*} b_{ik}^{\alpha*} L + a_{jq}^{\alpha} B_{kq}^{h*} a_{ik}^{\alpha*} R \right) - 2m_q m_j C_{12} \left(a_{jq}^{\alpha} B_{kq}^{h*} a_{ik}^{\alpha*} L + b_{jq}^{\alpha} A_{kq}^{h*} b_{ik}^{\alpha*} R \right) + \\ & + 4m_q m_k C_0 \left(b_{jq}^{\alpha} A_{kq}^{h*} a_{ik}^{\alpha*} L + a_{jq}^{\alpha} B_{kq}^{h*} b_{ik}^{\alpha*} R \right) + 2m_i m_k \left(C_{11} + C_0\right) \left(b_{jq}^{\alpha} B_{kq}^{h*} b_{ik}^{\alpha*} L + a_{jq}^{\alpha} A_{kq}^{h*} a_{ik}^{\alpha*} R \right) + \\ & -2m_j m_k \left(C_{12} + C_0\right) \left(a_{jq}^{\alpha} A_{kq}^{h*} a_{ik}^{\alpha*} L + b_{jq}^{\alpha} B_{kq}^{h*} b_{ik}^{\alpha*} R \right) \Big\} u_i, \end{aligned} \tag{C.6}$$

where $C = C\left(m_k^2, m_\alpha^2, m_q^2, m_i^2, m_j^2, m_h^2\right)$.

$$\begin{aligned} M_7 = \frac{-i\bar{u}_j}{16\pi^2} g_{\alpha\beta h}^{3h} \Big[& m_k C_0 \left(A_{jk}^{\beta} B_{ik}^{\alpha*} L + B_{jk}^{\beta} A_{ik}^{\alpha*} R \right) - m_j C_{12} \left(B_{jk}^{\beta} B_{ik}^{\alpha*} L + A_{jk}^{\beta} A_{ik}^{\alpha*} R \right) + \\ & + m_i \left(-C_{11} + C_{12}\right) \left(A_{jk}^{\beta} A_{ik}^{\alpha*} L + B_{jk}^{\beta} B_{ik}^{\alpha*} R \right) \Big] u_i, \end{aligned} \tag{C.7}$$

where $C = C\left(m_k^2, m_\alpha^2, m_\beta^2, m_i^2, m_h^2, m_j^2\right)$.

$$\begin{aligned} M_8 = \frac{-i\bar{u}_j}{16\pi^2} g_{\alpha\beta h}^{vvh} \Big[& 4m_k C_0 \left(b_{jk}^{\beta} a_{ik}^{\alpha*} L + a_{jk}^{\beta} b_{ik}^{\alpha*} R \right) + 2m_i \left(C_{11} - C_{12}\right) \left(b_{jk}^{\beta} b_{ik}^{\alpha*} L + a_{jk}^{\beta} a_{ik}^{\alpha*} R \right) + \\ & + 2m_j C_{12} \left(a_{jk}^{\beta} a_{ik}^{\alpha*} L + b_{jk}^{\beta} b_{ik}^{\alpha*} R \right) \Big] u_i, \end{aligned} \tag{C.8}$$

where $C = C\left(m_k^2, m_\alpha^2, m_\beta^2, m_i^2, m_h^2, m_j^2\right)$.

$$\begin{aligned} M_9 = \frac{i\bar{u}_j}{16\pi^2} g_{\beta\alpha h}^{vhh} \Big[& \left(\tilde{C}_0 + 2m_i^2 C_{11} + m_j^2 C_{12} - 2m_h^2 C_{12} \right) \left(b_{jk}^{\beta} B_{ik}^{\alpha*} L + a_{jk}^{\beta} A_{ik}^{\alpha*} R \right) + \\ & - m_i m_j \left(C_{12} + C_{11}\right) \left(a_{jk}^{\beta} A_{ik}^{\alpha*} L + b_{jk}^{\beta} B_{ik}^{\alpha*} R \right) + m_j m_k \left(C_0 - C_{12}\right) \left(a_{jk}^{\beta} B_{ik}^{\alpha*} L + b_{jk}^{\beta} A_{ik}^{\alpha*} R \right) + \\ & + m_i m_k \left(C_{12} - C_{11} - 2C_0\right) \left(b_{jk}^{\beta} A_{ik}^{\alpha*} L + a_{jk}^{\beta} B_{ik}^{\alpha*} R \right) \Big] u_i, \end{aligned} \tag{C.9}$$

where $C = C\left(m_k^2, m_\alpha^2, m_\beta^2, m_i^2, m_h^2, m_j^2\right)$.

$$\begin{aligned} M_{10} = \frac{i\bar{u}_j}{16\pi^2} g_{\alpha\beta h}^{vhh} \Big[& \left(-\tilde{C}_0 + m_i^2 \left(C_{12} - C_{11}\right) - 2m_j^2 C_{11} - 2m_h^2 \left(C_{12} - C_{11}\right) \right) \left(A_{jk}^{\beta} a_{ik}^{\alpha*} L + B_{jk}^{\beta} b_{ik}^{\alpha*} R \right) + \\ & + m_i m_j \left(2C_{11} - C_{12}\right) \left(B_{jk}^{\beta} b_{ik}^{\alpha*} L + A_{jk}^{\beta} a_{ik}^{\alpha*} R \right) + m_j m_k \left(C_{12} + 2C_0\right) \left(B_{jk}^{\beta} a_{ik}^{\alpha*} L + A_{jk}^{\beta} b_{ik}^{\alpha*} R \right) + \\ & + m_i m_k \left(C_{11} - C_{12} - C_0\right) \left(A_{jk}^{\beta} b_{ik}^{\alpha*} L + B_{jk}^{\beta} a_{ik}^{\alpha*} R \right) \Big] u_i, \end{aligned} \tag{C.10}$$

where $C = C\left(m_k^2, m_\alpha^2, m_\beta^2, m_i^2, m_h^2, m_j^2\right)$.

Appendix D

Definition of the n-point integral functions

We present here the definitions for 1-loop scalar, vector and tensor integrals:

$$B_0; B_\mu\left(m_1^2, m_2^2, p^2\right) = \int \frac{d^4k}{i\pi^2} \frac{1; k_\mu}{\left[k^2 - m_1^2\right]\left[(k+p)^2 - m_2^2\right]}, \tag{D.1}$$

$$C_0; C_\mu; C_{\mu\nu}; \tilde{C}_0\left(m_1^2, m_2^2, m_3^2, p_1^2, p_2^2\right) = \int \frac{d^4k}{i\pi^2} \frac{1; k_\mu; k_{\mu\nu}; k^2}{\left[k^2 - m_1^2\right]\left[(k+p_1)^2 - m_2^2\right]\left[(k+p_1+p_2)^2 - m_3^2\right]}, \tag{D.2}$$

$$\begin{aligned} \mathrm{B}_\mu &= p_\mu \mathrm{B}_1, \\ \mathrm{C}_\mu &= p_{1\mu}\mathrm{C}_{11} + p_{2\mu}\mathrm{C}_{12}, \\ \mathrm{C}_{\mu\nu} &= p_{1\mu}p_{1\nu}\mathrm{C}_{21} + p_{2\mu}p_{2\nu}\mathrm{C}_{22} + \{p_1 p_2\}_{\mu\nu}\mathrm{C}_{23} + g_{\mu\nu}\mathrm{C}_{24}, \end{aligned} \tag{D.3}$$

where $\{ab\}_{\mu\nu} \equiv a_\mu b_\nu + a_\nu b_\mu$.

Appendix E

Higgs width calculation

In this section we give the formulae that we used in calculating the Higgs width. The main contributions to the total width Γ^{tot} are:

$$\Gamma^{tot} = \Gamma^{h\rightarrow\bar{q}q} + \Gamma^{h\rightarrow VV} + \Gamma^{h\rightarrow H_iH_j} + \Gamma^{h\rightarrow VH}. \tag{E.1}$$

Only leading order values were used. The decay products are all taken to be on-shell, and their secondary decay products are not taken into account. Each contribution of $h \rightarrow x + y$ was calculated above the threshold: $m_h > m_x + m_y$. The vertices are defined here as in Fig. B.1.
The leading order value of $h \rightarrow \bar{q}q$ is [5]:

$$\Gamma\left(h \rightarrow \bar{q}q\right) = \frac{N_c A_{hqq}^2}{8\pi} m_h \left(1 - \frac{4m_q^2}{m_h^2}\right)^{\frac{3}{2}}, \tag{E.2}$$

where $A_{hqq} = -\frac{gm_q}{2m_W}\frac{\cos\alpha}{\cos\beta}; \frac{gm_q}{2m_W}\frac{\sin\alpha}{\cos\beta}$ is the quarks coupling to $H^0; h^0$, respectively, and $N_c = 3$ is the color factor, as mentioned above. We also give explicitly the width for the process $h^0 \rightarrow \bar{b}b$ in the T2HDM for $\alpha = \beta$:

$$\Gamma\left(h^0 \rightarrow \bar{b}b\right) = \frac{3g^2m_b^2}{32\pi m_W^2} m_{h^0} \tan^2\beta \left(1 - \frac{4m_b^2}{m_{h^0}^2}\right)^{\frac{3}{2}}. \tag{E.3}$$

The leading order value of $h \rightarrow W^+W^-$ is [5]:

$$\Gamma\left(h \rightarrow W^+W^-\right) = \frac{g_{hWW}^2 m_h^3}{64\pi m_W^4} \left(1 - x\right)^{\frac{1}{2}} \left(1 - x + \frac{3}{4}x^2\right), \tag{E.4}$$

where $g_{hWW} = gm_W \cos\left(\beta - \alpha\right); gm_W \sin\left(\beta - \alpha\right)$ is the W^+W^- coupling to $H^0; h^0$, respectively, and $x = \frac{4m_W^2}{m_h^2}$.
The leading order value of $h \rightarrow Z^0Z^0$ is [5]:

$$\Gamma\left(h \rightarrow Z^0Z^0\right) = \frac{g_{hZZ}^2 m_h^3 \cos^4\theta_W}{32\pi m_W^4} \left(1 - x\right)^{\frac{1}{2}} \left(1 - x + \frac{3}{4}x^2\right), \tag{E.5}$$

where $g_{hZZ} = \frac{gm_Z}{\cos\theta_W}\cos\left(\beta - \alpha\right); \frac{gm_Z}{\cos\theta_W}\sin\left(\beta - \alpha\right)$ is the Z^0Z^0 coupling to $H^0; h^0$, respectively, and $x = \frac{4m_Z^2}{m_h^2}$.
Since the couplings $W^+W^-h^0$ and $Z^0Z^0h^0$ are both $\propto \sin\left(\beta - \alpha\right)$ (as we have shown in table B.2), then by choosing $\alpha = \beta$, the widths of the processes $h^0 \rightarrow W^+W^-$ and $h^0 \rightarrow Z^0Z^0$ are both reduced to zero.

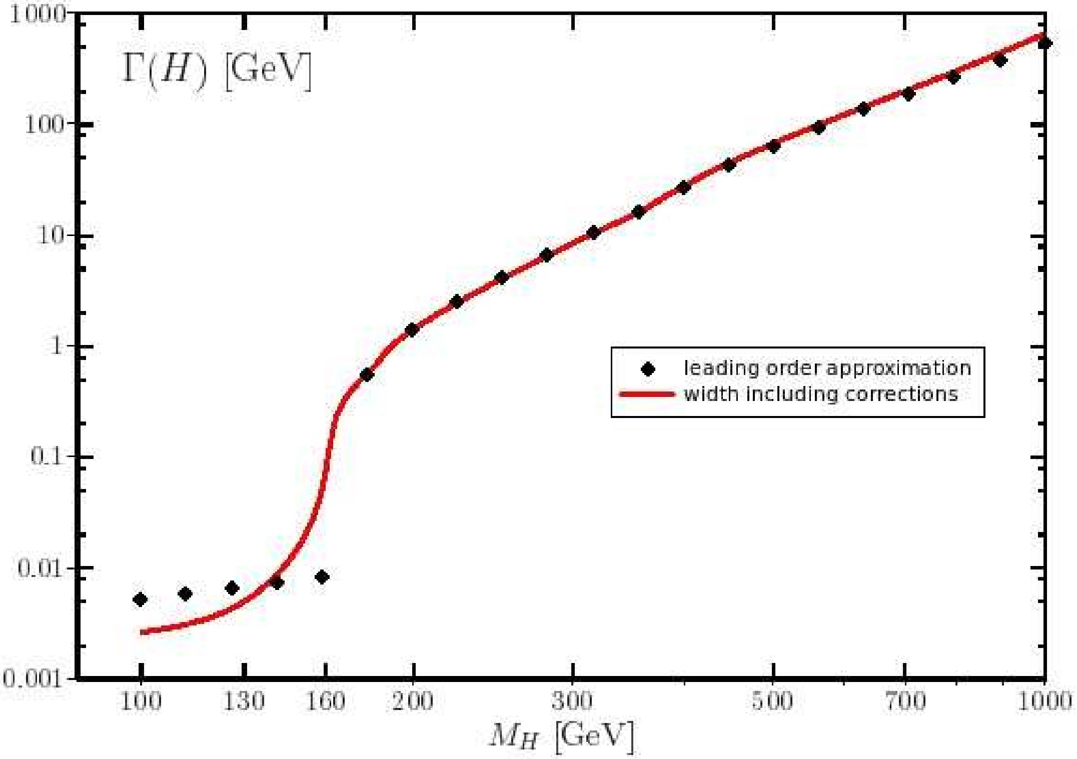

Figure E.1: The total width of the SM Higgs: leading order approximation compared to corrected width of [16].

The leading order value of $h \to H_i H_j$ (where H_i and H_j are any two scalars) is:

$$\Gamma\left(h \to H_i H_j\right) = \frac{g^2_{hH_iH_j}}{16\pi m_h} \lambda^{\frac{1}{2}} \left(1, \frac{m^2_{H_i}}{m^2_h}, \frac{m^2_{H_j}}{m^2_h}\right), \tag{E.6}$$

where $g_{hH_iH_j}$ is the triple Higgs coupling hH_iH_j.
The leading order value of $h \to VH$ (where $VH = W^+H^-$ or $Z^0 +$ neutral scalar) is:

$$\Gamma\left(h \to VH\right) = \frac{g^2_{VHh} m^2_V}{16\pi m_h} \lambda^{\frac{1}{2}} \left(1, \frac{m^2_V}{m^2_h}, \frac{m^2_H}{m^2_h}\right) \lambda \left(1, \frac{m^2_h}{m^2_V}, \frac{m^2_H}{m^2_V}\right), \tag{E.7}$$

where g_{hVH} is the vector-scalar-scalar coupling VHh. This contribution can be important, as stated in Sec. 4.4.
In order to demonstrate the error introduced by including only leading terms in the Higgs width calculation, we give in Fig. E.1 the total SM Higgs width as calculated in this work compared to the width of [16] which includes higher-order corrections.
As can be seen, below the WW threshold (at about 160 GeV) the values are different. In this mass range $b\bar{b}$ decay dominates, and corrections have a large impact. However, this mass range is also below the $h \to \bar{t}c$ threshold. On the other hand, above the WW threshold the values are very similar, and corrections have a small impact, and so the use of leading order approximation can be justified.

Appendix F

Cancellation of divergences in the 1-loop amplitude

Some of the 1-loop Feynman diagrams have a divergent part. These divergent parts cancel, since this is a leading-order calculation and, therefore, there is no renormalization.
This cancellation is also important as a means of checking the self consistency of the calculation. We define $\varepsilon = 4 - d$, where $d \to 4$ is the number of dimensions. As $\varepsilon \to 0$, some n-point integrals will have a term proportional to $\frac{1}{\varepsilon}$. These are summarized below:

$$\begin{aligned} B_0 &\sim -2\frac{1}{\varepsilon} \quad , \qquad & C_{24} &\sim -\frac{1}{2}\frac{1}{\varepsilon}, \\ B_1 &\sim 1\frac{1}{\varepsilon} \quad , \qquad & \tilde{C}_0 &\sim -2\frac{1}{\varepsilon}. \end{aligned} \tag{F.1}$$

The parts of the Feynman diagrams proportional to $\frac{1}{\varepsilon}$ were collected below. Only the parts of the diagrams with a left projection operator are given, while the right-handed parts are subject to a similar cancellation. The Feynman diagrams were shown in Fig. 4.1.

$$\begin{aligned} M_{1L}^{\infty l=j} &= \frac{-1}{m_i^2 - m_l^2}\left[-2m_k\left(m_l B_{lj}^{H^0 *} A_{lk}^{\alpha} B_{ik}^{\alpha *} + m_i B_{lj}^{H^0 *} B_{lk}^{\alpha} A_{ik}^{\alpha *}\right) - \right. \\ &\qquad \left. - \, m_i\left(m_l B_{lj}^{H^0 *} A_{lk}^{\alpha} A_{ik}^{\alpha *} + m_i B_{lj}^{H^0 *} B_{lk}^{\alpha} B_{ik}^{\alpha *}\right)\right], \\ M_{2L}^{\infty l=i} &= \frac{-1}{m_j^2 - m_l^2}\left[-2m_k\left(m_l A_{jk}^{\alpha} B_{lk}^{\alpha *} B_{il}^{H^0 *} + m_j B_{jk}^{\alpha} A_{lk}^{\alpha *} B_{il}^{H^0 *}\right) - \right. \\ &\qquad \left. - \, m_j\left(m_l B_{jk}^{\alpha} B_{lk}^{\alpha *} B_{il}^{H^0 *} + m_j A_{jk}^{\alpha} A_{lk}^{\alpha *} B_{il}^{H^0 *}\right)\right], \\ M_{3L}^{\infty l=j} &= \frac{1}{m_i^2 - m_l^2}\left[-8m_k\left(m_l B_{lj}^{H^0 *} b_{lk}^{\alpha} a_{ik}^{\alpha *} + m_i B_{lj}^{H^0 *} a_{lk}^{\alpha} b_{ik}^{\alpha *}\right) - \right. \\ &\qquad \left. - \, 2m_i\left(m_l B_{lj}^{H^0 *} b_{lk}^{\alpha} b_{ik}^{\alpha *} + m_i B_{lj}^{H^0 *} a_{lk}^{\alpha} a_{ik}^{\alpha *}\right)\right], \\ M_{4L}^{\infty l=i} &= \frac{1}{m_j^2 - m_l^2}\left[-8m_k\left(m_l b_{jk}^{\alpha} a_{lk}^{\alpha *} B_{il}^{H^0 *} + m_j a_{jk}^{\alpha} b_{lk}^{\alpha *} B_{il}^{H^0 *}\right) - \right. \\ &\qquad \left. - \, 2m_j\left(m_l a_{jk}^{\alpha} a_{lk}^{\alpha *} B_{il}^{H^0 *} + m_j b_{jk}^{\alpha} b_{lk}^{\alpha *} B_{il}^{H^0 *}\right)\right], \end{aligned}$$

$$\begin{aligned}
M_{5L}^{\infty q=k} &= 2A^{\alpha}_{jq}A^{H^0*}_{kq}B^{\alpha*}_{ik}, \\
M_{6L}^{\infty q=k} &= -8b^{\alpha}_{jq}B^{H^0*}_{kq}a^{\alpha*}_{ik}, \\
M_{7L}^{\infty} &= 0, \\
M_{8L}^{\infty} &= 0, \\
M_{9L}^{\infty} &= -2g^{vhh}_{\beta\alpha H^0}b^{\beta}_{jk}B^{\alpha*}_{ik}, \\
M_{10L}^{\infty} &= 2g^{vhh}_{\alpha\beta H^0}A^{\beta}_{jk}a^{\alpha*}_{ik}.
\end{aligned} \tag{F.2}$$

After inserting the Feynman rules of the T2HDM, we were able to show that the terms proportional to $\frac{1}{\varepsilon}$ cancel as shown below:

$$\begin{aligned}
& M_1^{\infty} + M_2^{\infty} + M_5^{\infty} = 0, \\
& M_3^{\infty} + M_4^{\infty} = 0, \\
& M_6^{\infty} = 0, \\
& M_7^{\infty} = 0, \\
& M_8^{\infty} = 0, \\
& M_9^{\infty} = 0, \\
& M_{10}^{\infty} = 0.
\end{aligned} \tag{F.3}$$

This cancellation was also verified numerically in the FORTRAN code.

Bibliography

[1] A. Das, C. Kao, “A two Higgs doublet model for the top quark”, Phys. Lett. B**372**, 106 (1996), arXiv:hep-ph/9511329

[2] E. Lunghi, A. Soni, “Footprints of the Beyond in flavor physics: Possible role of the Top Two Higgs Doublet Model”, FERMILAB-PUB-07-315-T (2007), arXiv:hep-ph/0707.0212

[3] G. Eilam, J.L. Hewett, A. Soni, “Rare decays of the top quark in the standard and two Higgs doublet models”, Phys. Rev. D**44**, 1473 (1991), see also: Erratum, Phys. Rev. D**59**:039901 (1999); B. Mele, S. Petrarca, A. Soddu, ”A New evaluation of the $t \to cH$ decay width in the standard model”, Phys. Lett. B**435**, 401 (1998), arXiv:hep-ph/9805498

[4] A. Arhrib, “Higgs bosons decay into bottom-strange in two Higgs Doublets Models”, Phys. Lett. B**612**, 263 (2005), arXiv:hep-ph/0409218

[5] J. F. Gunion, H. E. Haber, G. Kane, S. Dawson, “The Higgs Hunter’s Guide”, Addison-Wesley (1990); see also: Errata, SCIPP-92-58 (1992), arXiv:hep-ph/9302272

[6] H. Georgi, “A model of soft CP violation”, Hadronic J. **1**, 155 (1978)

[7] D. Atwood, S. Bar-Shalom, G. Eilam, A. Soni, ”Flavor changing Z-decays from scalar interactions at a Giga-Z Linear Collider”, Phys. Rev. D**66**:093005 (2002), arXiv:hep-ph/0203200

[8] G.-H. Wu, A. Soni, “Novel CP-violating effects in B decays from a charged Higgs boson in a two-Higgs-doublet model for the top quark”. Phys. Rev. D**62**:056005 (2000), arXiv:hep-ph/9911419

[9] D. Atwood, S. Bar-Shalom, G. Eilam, A. Soni, ”Three heavy jet events at hadron colliders as a sensitive probe of the Higgs sector”, Phys. Rev. D**69**:033006 (2004), arXiv:hep-ph/0309016

[10] K. Agashe, G. Perez, A. Soni, ”Collider Signals of Top Quark Flavor Violation from a Warped Extra Dimension”, Phys. Rev. D**75**:015002 (2007), arXiv:hep-ph/0606293; L. Randall and R. Sundrum, Phys. Rev. Lett. **83**, 3370 (1999), arXiv:hep-ph/9905221

[11] V.A. Miransky, M. Tanabashi, K. Yamawaki, ”Dynamical Electroweak Symmetry Breaking with Large Anomalous Dimension and t Quark Condensate”, Phys. Lett. B**221**, 177 (1989) ; R. S. Chivukula, B. Dobrescu, H. Georgi, C. T. Hill, ”Top quark seesaw theory of electroweak symmetry breaking”, Phys. Rev. D**59**, 075003, (1999), arXiv:hep-ph/9809470

[12] See e.g., G. Isidori, “Rare decays: theory vs. experiments”, Int. J. Mod. Phys. A**17**, 3078 (2002), arXiv:hep-ph/0110255; B. Mele, “Top quark rare decays in the standard model and beyond”, Proc. 14th Internat. Workshop HEP QFT (QFTHEP 99), 1999, arXiv:hep-ph/0003064

[13] J. Hisano, T. Moroi, K. Tobe, Masahiro Yamaguchi, T. Yanagida, ”Lepton flavor violation in the supersymmetric standard model with seesaw induced neutrino masses”, Phys. Lett. B**357**, 579 (1995), arXiv:hep-ph/9501407

[14] J.A. Aguilar-Saavedra, ”Top flavor-changing neutral interactions: Theoretical expectations and experimental detection”, Acta Phys. Polon. B**35**, 2695 (2004), arXiv:hep-ph/0409342; J.A. Aguilar-Saavedra, G.C. Branco, “Probing top flavor changing neutral scalar couplings at the CERN LHC”, Phys. Lett. B**495**, 347 (2000), arXiv:hep-ph/0004190

[15] S. Bejar, “Flavor changing neutral decay effects in models with two Higgs boson doublets: Applications to LHC Physics”, PhD thesis (2006), arXiv:hep-ph/0606138; S. Bejar, J. Guasch, J. Sola, “Loop Induced Flavor Changing Neutral Decays of the Top Quark in a General Two-Higgs-Doublet Model”, Nucl. Phys. B**600**, 21 (2001), arXiv:hep-ph/0011091

[16] A. Djouadi, ”The Anatomy of Electro-Weak Symmetry Breaking, Tome I: The Higgs boson in the Standard Model”, LPT-ORSAY-05-18 (2005), arXiv:hep-ph/0503172

[17] M. E. Peskin, D. V. Schroeder, "An introduction to quantum field theory", Perseus Books (1995)

[18] A. Bramon, E. Shabalin, “A relation between the electric dipole moments of the neutron and the electron in two-Higgs-doublet models”, Phys. Lett. B**404**, 115 (1997)

[19] K. Kiers, A. Soni, G.-H. Wu, “CP violation in a two-Higgs doublet model for the top quark: $B \to \Psi K_S$”, Phys. Rev. D**59**:096001 (1999), arXiv:hep-ph/9810552

[20] K. Kiers, A Soni, G.-H. Wu, “Direct CP violation in radiative b decays in and beyond the Standard Model”. Phys. Rev. D**62**:116004 (2000), arXiv:hep-ph/0006280

[21] Heavy Flavor Averaging Group (HFAG) Collaboration (E. Barberio et al.), “Averages of b-hadron properties at the end of 2006”, (Apr. 2007), arXiv:hep-ex/0704.3575

[22] L.-X. Lu, Z.-J. Xiao, “$B^0_{s(d)} - \bar{B}^0_{s(d)}$ mixing and new physics effects in a top quark two-Higgs doublet model”, NJNU-TH-06-30 (2006), arXiv:hep-ph/0609279

[23] L.-X. Lu, Z.-J. Xiao, ”The Neutral Higgs Effects on Rare Decays $B \to X_S l^+ l^-$ in T2HDM”, arXiv:hep-ph/0611252 (2006); Z.-J. Xiao, L.-X. Lu, “$B \to X_S l^+ l^-$ decay in a Top quark two-Higgs-doublet model”, Phys. Rev. D**74**:034016 (2006), arXiv:hep-ph/0605076

[24] G. J. van Oldenborgh, “FF: A Package to evaluate one loop Feynman diagrams”, NIKHEF-H-90-15 (1990); Comput. Phys. Commun. **66**, 1 (1991); download: http://www.xs4all.nl/~gjvo/FF.html

[25] A. Arhrib, “Top and Higgs Flavor Changing Neutral Couplings in two Higgs Doublets Model”, Phys. Rev. D**72**:075016 (2005), arXiv:hep-ph/0510107

[26] D. Atwood, L. Reina, A. Soni, ”Phenomenology of two Higgs doublet models with flavor changing neutral currents”, Phys. Rev. D**55**, 3156 (1997), arXiv:hep-ph/9609279

[27] W.-M. Yao et al. (Particle Data Group), J. Phys. G**33**, 1 (2006) and 2007 partial update for the 2008 edition (URL: http://pdg.lbl.gov)

[28] A. Djouadi, ”The Anatomy of Electro-Weak Symmetry Breaking, Tome II: The Higgs bosons in the Minimal Supersymmetric Model”, LPT-ORSAY-05-18 (2005), arXiv: hep-ph/0503173

[29] C.R. Das, M.K. Parida, ”New formulae and predictions for running fermion masses at higher scales in SM, 2 HDM, and MSSM”, Eur. Phys. J. C**20**, 121 (2001), arXiv:hep-ph/0010004